Detailed spectroscopy and γ-γ angular correlation measurements of ^{122}Xe

B. Jigmeddorj,[1,2,*] P. E. Garrett,[1,3] L. Próchniak,[4] A. J. Radich,[1] C. Andreoiu,[5] G. C. Ball,[6] T. Bruhn,[5,6] D. S. Cross,[5] A. B. Garnsworthy,[6] B. Hadinia,[1,†] S. F. Hicks,[7,8] M. Moukaddam,[6,‡] J. Park,[6,9,§] J. L. Pore,[5,‖] M. M. Rajabali,[6,¶] E. T. Rand,[1,#] U. Rizwan,[5] C. E. Svensson,[1] P. Voss,[5,**] Z. M. Wang,[5,6] J. L. Wood,[10] and S. W. Yates[8]

[1]*Department of Physics, University of Guelph, Guelph, Ontario N1G2W1, Canada*
[2]*School of Natural Science, Laurentian University, Sudbury, Ontario P3E2C6, Canada*
[3]*Instituut voor Kernen Stralingsfysica, KU Leuven, B-3001 Leuven, Belgium*
[4]*Heavy Ion Laboratory, University of Warsaw, PL 02-093 Warsaw, Poland*
[5]*Department of Chemistry, Simon Fraser University, Burnaby, British Columbia V5A1S6, Canada*
[6]*TRIUMF, 4004 Wesbrook Mall, Vancouver, British Columbia V6T2A3, Canada*
[7]*Department of Physics, University of Dallas, Irving, Texas 75062-4736, USA*
[8]*Departments of Chemistry and Physics & Astronomy, University of Kentucky, Lexington, Kentucky 40506-0055, USA*
[9]*University of British Columbia, Vancouver, British Columbia V6T2A3, Canada*
[10]*School of Physics, Georgia Institute of Technology, Atlanta, Georgia 30332-0430, USA*

(Received 2 February 2024; revised 27 March 2024; accepted 2 July 2024; published 8 August 2024)

Excited states of ^{122}Xe populated via β^+ and electron capture (EC) decay of ^{122}Cs have been studied with γ-ray spectroscopy using the 8π spectrometer at the TRIUMF Isotope Separator and Accelerator facility. Two sets of data were collected to optimize the signal-to-background ratio for decays of the ground ($t_{1/2} = 21.2$ s) and isomeric ($t_{1/2} = 3.7$ min) states of ^{122}Cs. The data collected have enabled the observation of 520 transitions and 191 levels, including eight new excited 0^+ states in ^{122}Xe. The γ-γ angular correlations have been analyzed that permitted the assignment or restriction of the spins for 66 levels. The $E2/M1$ multipolarity mixing ratios for 38 γ-ray transitions were also extracted from these analyses. Low-spin members of the 0_2^+, 0_3^+, 0_4^+, and $K^\pi = 4^+$ bands are assigned, as well as suggested $K^\pi = 2_2^+$ and $K^\pi = 2_3^+$ bandheads. Combined with previous results for high-spin states, rotational bands built on a newly assigned $K^\pi = 3_1^-$ state and its 4_1^- signature partner, the 5_2^- and its 6_2^- signature partner, are suggested. The results for the positive-parity bands are compared with a model using a general Bohr Hamiltonian derived from a mean-field theory based on the UNEDF0 energy-density functional that displays good overall agreement.

DOI: 10.1103/PhysRevC.110.024305

I. INTRODUCTION

The Xe isotopes are currently the subject of much interest since they are candidates for the observation of neutrinoless double β decay ($0\nu\beta\beta$). While ^{136}Xe is a leading contender, and actively used in searches (see, e.g., Refs. [1,2]), other isotopes such as ^{124}Xe have been advocated [3], and ^{130}Xe is the daughter of ^{130}Te that is used as an active detector material [4,5]. As outlined in detail elsewhere [6,7], should a $0\nu\beta\beta$ signal be detected, in order to extract the neutrino masses the nuclear matrix element for the process must be known. This has proved to be a challenge since different calculations and theoretical approaches yield differences in the matrix elements by factors of 2–4 [7], or approaching an order of magnitude in the transition rate. A key element for the calculations is a good reproduction of the nuclear structure of the states, as it has been shown that there is a strong dependence of the value of the nuclear matrix element on the change in deformation between the parent and daughter [7].

The Xe isotopes have been considered in a variety of structure models, although, away from the closed $N = 82$ shell (^{136}Xe), these are mostly based on collective degrees of freedom. Brentano *et al.* [8] considered ^{120}Xe and ^{124}Xe as good examples of the O(6) symmetry of the interacting boson model (IBM), analogous to the γ-soft limit of the Bohr model. However, when more precise tests were made [9,10] of ^{124}Xe, for example, it was found that the O(6) symmetry was badly broken but it appeared that O(5) was preserved. It was also suggested [11] that ^{128}Xe displayed characteristics of the E(5) symmetry—a symmetry of the Bohr model for

*Contact author: bjigmeddorj@laurentian.ca
†Present address: McMaster University, Hamilton, ON, Canada.
‡Present address: University of Surrey, Guildford, UK.
§Present address: Center for Exotic Nuclear Studies, Institute for Basic Science, 34126 Daejeon, Korea.
‖Present address: Lawrence Berkeley National Laboratory, USA.
¶Present address: Tennessee Technological University, TN, USA.
#Present address: Canadian Nuclear Laboratories, Chalk River, ON, Canada.
**Present address: Albion College, Michigan, USA.

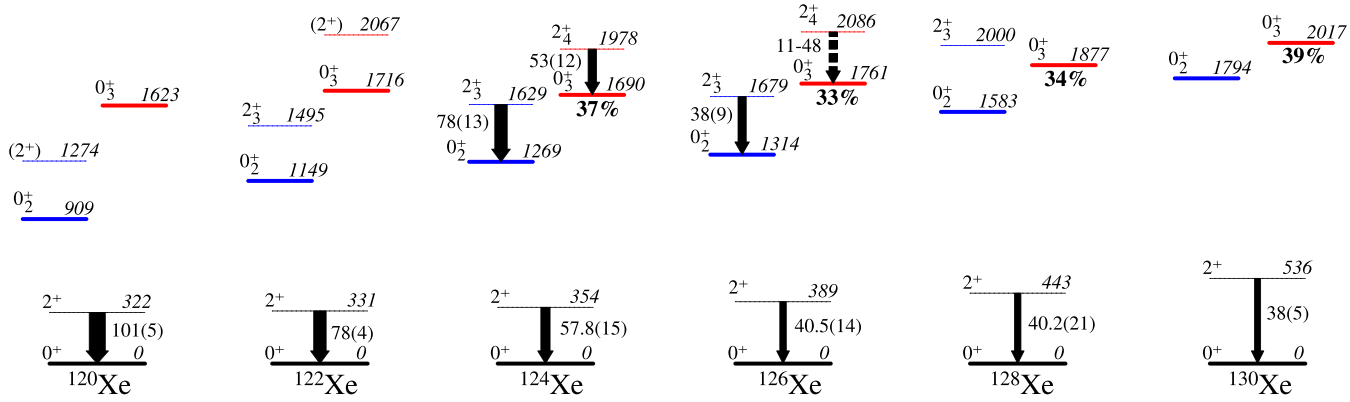

FIG. 1. Systematics of the low-lying excited 0^+ states for the $^{120-130}$Xe isotopes. The ratios of population cross sections to excited 0^+ states relative to the ground states in the Te(^{3}He, n) reactions [15], expressed as a percentage, are shown below the levels. Also shown are the in-band $B(E2; 2^+ \rightarrow 0^+)$ values, in W.u., where known [16–22].

the critical point of the transition from spherical vibrator to deformed γ-soft rotor—but this interpretation was refuted using results from Coulomb excitation studies [12]. Other theoretical approaches applied to the Xe isotopes include the dynamic pairing plus quadrupole (DPPQ) model [13], as well as beyond mean field approaches [14].

Potential proton pairing vibration states in $^{124-132}$Xe isotopes were observed by Alford *et al.* [15] using the Te(^{3}He, n) reactions. The results are shown in Fig. 1, where it can be seen that the 0_3^+ states have very large cross sections relative to that of the ground states, ranging from 33% (^{126}Xe) to 39% (^{130}Xe), indicating a character of a proton pairing vibration. While the two-proton-transfer reactions populating ^{120,122}Xe have not been performed, from the smooth evolution of the excitation energies it is likely that their 0_3^+ states have the same proton-pairing character as in the heavier Xe isotopes. Also shown in Fig. 1 are the known in-band absolute $B(E2; 2^+ \rightarrow 0^+)$ values for the 0^+ bands. A remarkable drop in the $B(E2)$ value is observed for the $2_3^+ \rightarrow 0_2^+$ transition in ^{126}Xe, becoming approximately 50% of that of the corresponding transition in ^{124}Xe. The 0_3^+ pairing vibrational states are influenced by proton subshell gaps which could possibly lead to shape coexistence [23]. This potential situation was tested using results from a β-decay study of ^{124}Xe [19] which, when combined with the results of a previous Coulomb excitation work [10], permitted the $\langle Q^2 \rangle$ invariant quantity to be extracted more precisely for the 0_1^+, 0_2^+, and 0_3^+ states. It was found that the ground and 0_3^+ states had nearly identical magnitudes of deformation β, with 0.23(1) and 0.22(2), respectively, while that of the 0_2^+ state was substantially larger with $\beta = 0.29(2)$. Thus, this situation is unlike the Cd isotopes where there are large two-proton-transfer cross sections to the shape-coexisting intruder bandheads [24,25]. The trend in deformation in ^{124}Xe was in conflict with the IBM results that predicted a monotonically decreasing β, while the DPPQ model [13] overpredicted the values for the 0_2^+ and 0_3^+ states, although the trend is somewhat reproduced [19,26]. A caveat to these calculations, however, is that the observed 0_3^+ state lies outside their model spaces if a proton-pairing vibration interpretation is correct. This situation was recently remedied within the context of IBM calculations by Nomura *et al.* [27] through the addition of both $N-1$ and $N+1$ boson configurations, where N is the boson number for the system considered. Significant amplitudes of the pairing vibrational configurations were found for both the 0_2^+ and 0_3^+ states of ^{122}Xe, indicating that this configuration is the dominant component for the 0_2^+ state [27].

In the current work, results of an experiment to study the β^+ and electron capture (EC) decay of ^{122}Cs to ^{122}Xe are presented. The data collected expand the current ^{122}Xe level scheme considerably with new γ-ray branches and levels from γ-γ coincidence measurements. Owing to the high level of statistics collected during this experiment, it was possible to use γ-γ angular correlations to calculate mixing ratios for many γ-ray transitions and derive spin and parity assignments for many levels. The low-energy levels are organized in rotational bands, and the results are compared with beyond mean field calculations.

The analysis of the data from the experiment enabled us to observe 520 γ-ray transitions and 191 energy levels including eight new excited 0^+ states. Some initial results published on ^{122}Xe included the establishment of the 2^+ band members of the 0_2^+ and 0_3^+ bands with the observation of the $2_2^+ \rightarrow 0_2^+$ and $2_3^+ \rightarrow 0_3^+$ transitions [28]. Our second report on ^{122}Xe [29,30] confirmed the spins of the 0_3^+ state and the previously suggested 2^+ members of the 0_2^+ and 0_3^+ bands using angular correlation analysis. Results on low-lying excited states in ^{122}Xe were also briefly discussed in Ref. [31]. The present work represents the final analysis and supersedes these initial results.

II. EXPERIMENTAL DETAILS

The experiment to study the β^+/EC of ^{122}Cs was performed at the TRIUMF Isotope Separator and Accelerator (ISAC) facility located in Vancouver, BC, Canada. A 65-μA, 480-MeV proton beam from the TRIUMF main cyclotron was delivered to the ISAC facility and bombarded a thick $^{\text{nat}}$Ta foil target. Products of the spallation reaction diffused to the surface of the Ta target foils, were ionized with a Re surface-ion source, and passed through a magnetic mass separator that was set to select singly charged $A = 122$ ions. The high-intensity beam of 1.1×10^7 ions/s of ^{122}Cs in the

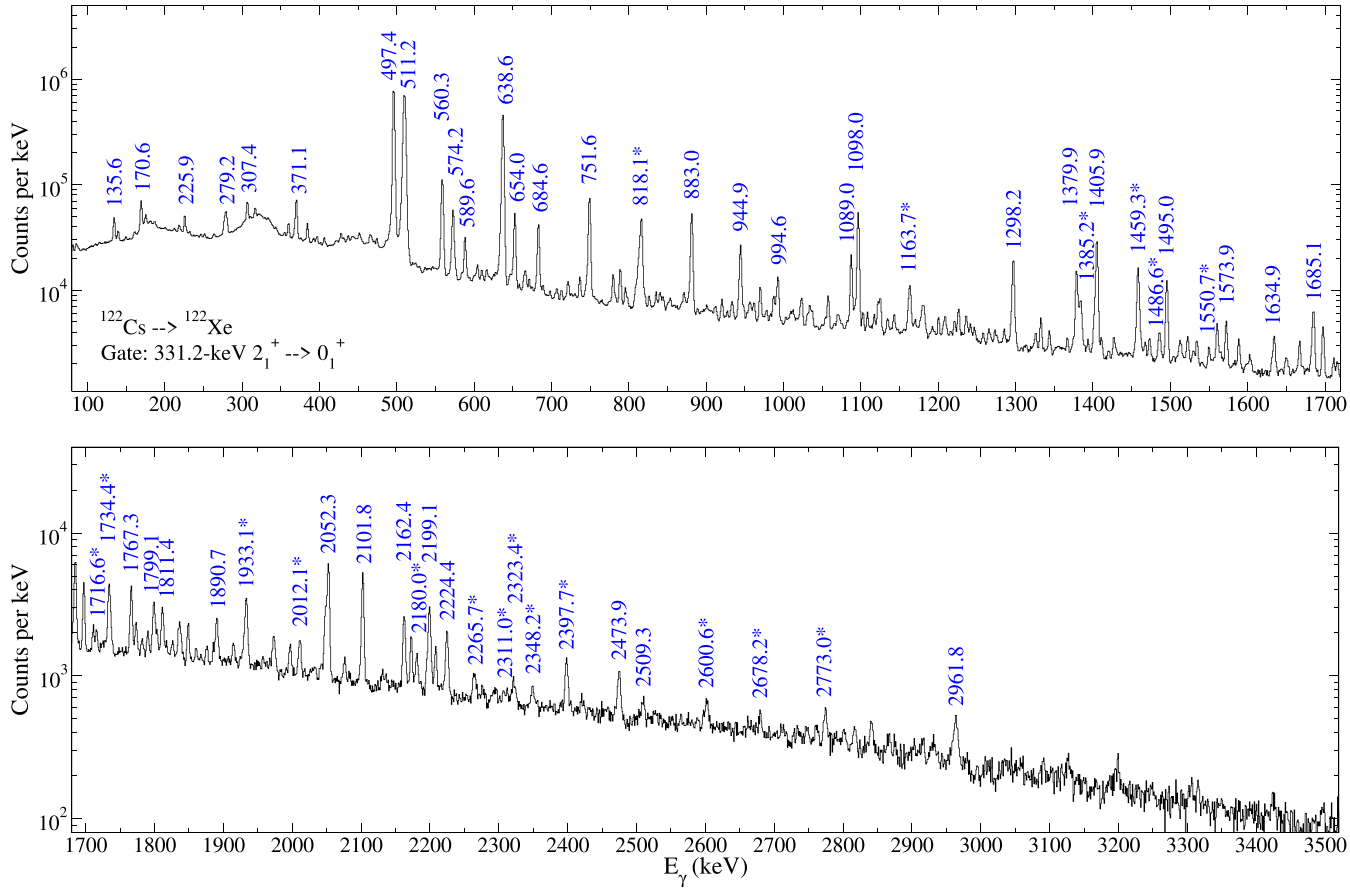

FIG. 2. Portion of the γ-ray spectrum observed from the long-cycle data with a coincidence condition placed on the 331.2 keV $2_1^+ \rightarrow 0_1^+$ γ ray. Some of the prominent γ rays observed are labeled with their energy in keV, and the γ rays used for an angular correlation analysis with the 331.2 keV γ ray are indicated by an asterisk.

1^+ ground state with a 21.2 s half-life, and 2.1×10^6 ions/s of ^{122}Cs in the $8^{(-)}$ isomeric state with a 3.7 minute half-life, was delivered to the center of the 8π γ-ray spectrometer [26,32–34] and implanted into a FeO-coated mylar tape. The 8π spectrometer consisted of twenty high-purity germanium (HPGe) detectors surrounded by bismuth-germanate (BGO) Compton-suppression shields. The average source-to-Ge-detector distance was approximately 14 cm. The five Si(Li) detectors of the PACES array for conversion-electron detection were positioned upstream and aligned to the beam-spot position. The average source-to-Si-detector distance was 3 cm. More details of the 8π spectrometer are given in Refs. [26,32], and PACES is described in Refs. [26,35]. The Ge-detector efficiencies were measured using standard radioactive sources of ^{133}Ba, ^{152}Eu, ^{56}Co, and ^{60}Co that were placed inside the vacuum chamber at the beam deposition location.

Two sets of data were collected in repeated cycles, labeled as "short" and "long" cycles. The short cycle consisted of a brief period of background collection (1.5 s), followed by a beam delivery of 20 s after which the beam was deflected and the decay was observed for a further 20 s. The tape was then moved such that the beam deposition spot was removed from the array and transported to a position within a shielded tape box. For the long cycles, the beam deposition and decay periods were adjusted to 450 and 450 s, respectively. Each set of data was collected in a mixed-trigger mode involving scaled-down γ-ray and e^- singles, and γ-γ and γ-e^- coincidences. The data were sorted into γ-ray and e^- spectra from the singles-trigger mode, and γ-γ and γ-e^- time-random-background subtracted coincidence matrices. Analyses of the γ-γ matrices and fitting of the spectra were performed with the RADWARE package [36]. While conversion e^- data were recorded during the experiment, unfortunately no significant new results could be extracted since the majority of the expected electron peaks were not observable above the backgrounds present in the Si(Li) detectors. Therefore, the results presented in this work are focused on the γ-ray data.

III. LEVEL SCHEME OF ^{122}Xe

The level scheme of ^{122}Xe has been dramatically expanded and is shown in the Supplemental Material [37]. The two sets of data collected in the short- and long-cycle durations favor the decays of the low-spin short-lifetime ground state and the longer-lived high-spin isomeric state, respectively. The level

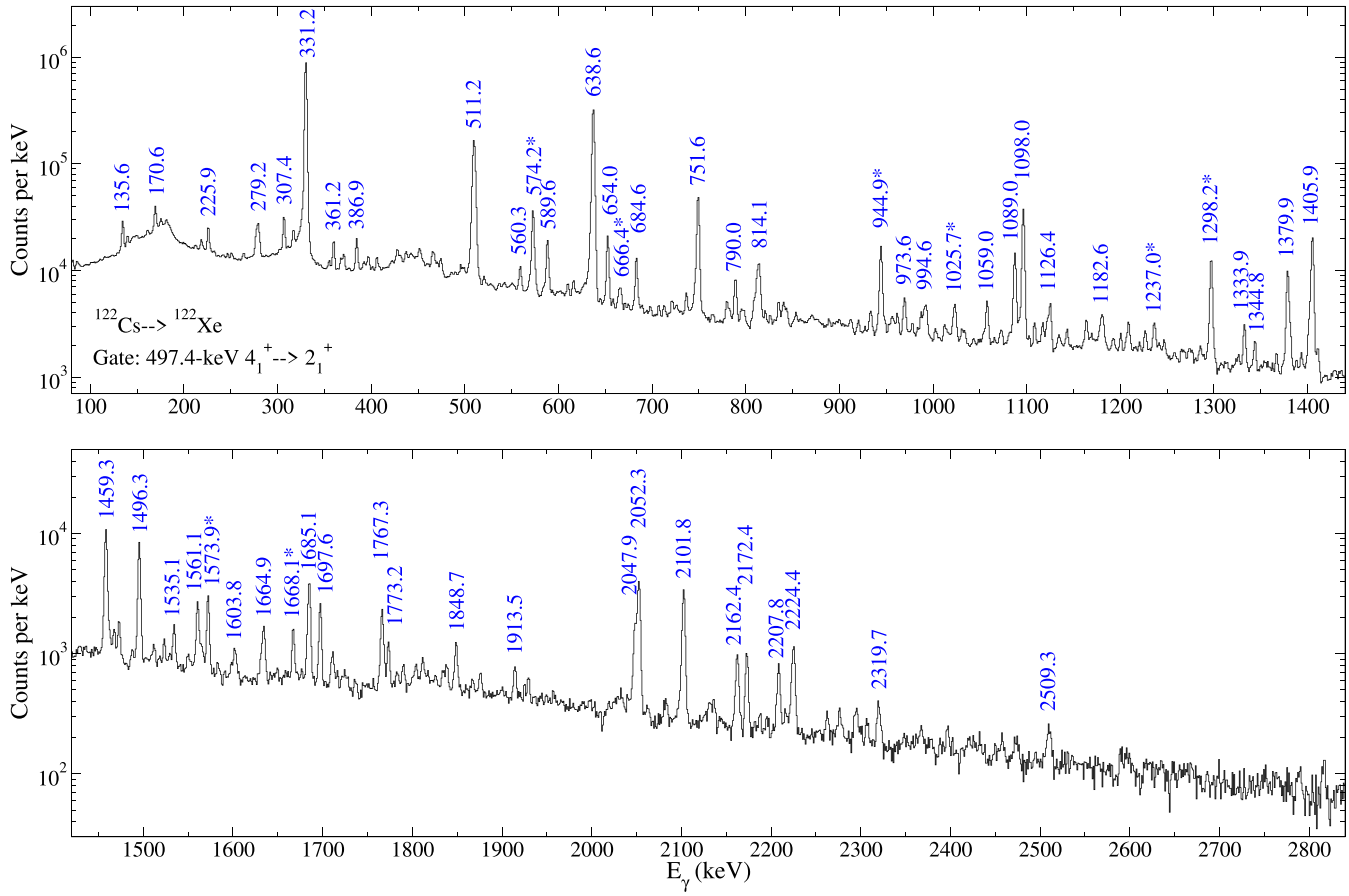

FIG. 3. Portion of the γ-ray spectrum observed from the long-cycle data with a coincidence condition placed on the 497.4 keV $4_1^+ \rightarrow 2_1^+$ γ ray. Some of the prominent γ rays observed are labeled with their energy in keV, and the γ rays used for an angular correlation analysis with the 497.4 keV γ ray are indicated by an asterisk.

scheme of ^{122}Xe was built primarily on analyses of γ-γ time-random-background-subtracted coincidence matrices.

A. Branching Ratios

The branching ratios were determined from the analysis of the γ-γ coincidence data using both gating from above, where feasible, and the gating from below technique as outlined in Refs. [38–40]. Figures 2–4 display portions of the γ-ray spectra obtained from the γ-γ coincidence matrices constructed from the long-cycle data, with coincidence conditions placed on the 331.2 keV $2_1^+ \rightarrow 0_1^+$ (Fig. 2), the 497.4 keV $4_1^+ \rightarrow 2_1^+$ (Fig. 3), and 843.2 keV $2_2^+ \rightarrow 0_1^+$ (Fig. 4) γ rays, respectively.

The number of counts in a coincidence peak, N_c, is given by

$$N_c = \mathcal{N} I_{\gamma_f} \epsilon_{\gamma_f} P_{\gamma_d} \epsilon_{\gamma_d} \epsilon_c \eta(\theta_{fd}), \tag{1}$$

where $\mathcal{N}$ is an overall normalization factor for a particular data set, I_{γ_f} is the γ-ray intensity for the feeding transition to a level, P_{γ_d} is the probability of the draining γ ray being emitted from the level, ϵ_γ is the γ-ray detection efficiency, ϵ_c accounts for the deviation of the relative detection efficiency from that determined using γ-ray singles source data due to the coincidence condition, which in principle depends on both the feeding and draining γ-ray energies, and $\eta(\theta_{fd})$ is the angular correlation correction factor for the particular pair of feeding and draining γ rays. Angular correlation effects are generally smaller than a few percent due to the symmetry of the 8π spectrometer [38] when all detectors are used. The γ-γ coincidence efficiency factor ϵ_c is generally most affected by the coincidence time conditions placed on the data, and care was taken in the selection of events with the very generous condition $|\Delta t_{\gamma\gamma}| \leqslant 230$ ns to account for time-walk effects for the low-energy transitions. Further, the high-degree of symmetry and similarity of the Ge detectors was such that the impact on the efficiency of an event in one detector, and the subsequent event in the remaining 19 detectors, is also minimized. Thus, ϵ_c was assumed to be 1. The validity of this assumption has been tested by branching ratios obtained using multiple gates and comparison with singles intensities in similar analyses carried out with other data sets (see, e.g., Ref. [40]). To generate the coincidence spectra, generally the gate was taken on the strongest draining transition from a level. Ignoring the common factor $\mathcal{N}$, intensities of the feeding transitions were obtained by dividing the peak areas by the γ-ray singles photopeak efficiencies of both the feeding and draining γ rays and the probability P_{γ_d} of the draining γ ray [for the present analysis, $P_{\gamma_d} = \mathrm{BR}(\gamma_d)$]. The γ-ray branching ratios $\mathrm{BR}(\gamma_f)$ were found by dividing the peak intensity

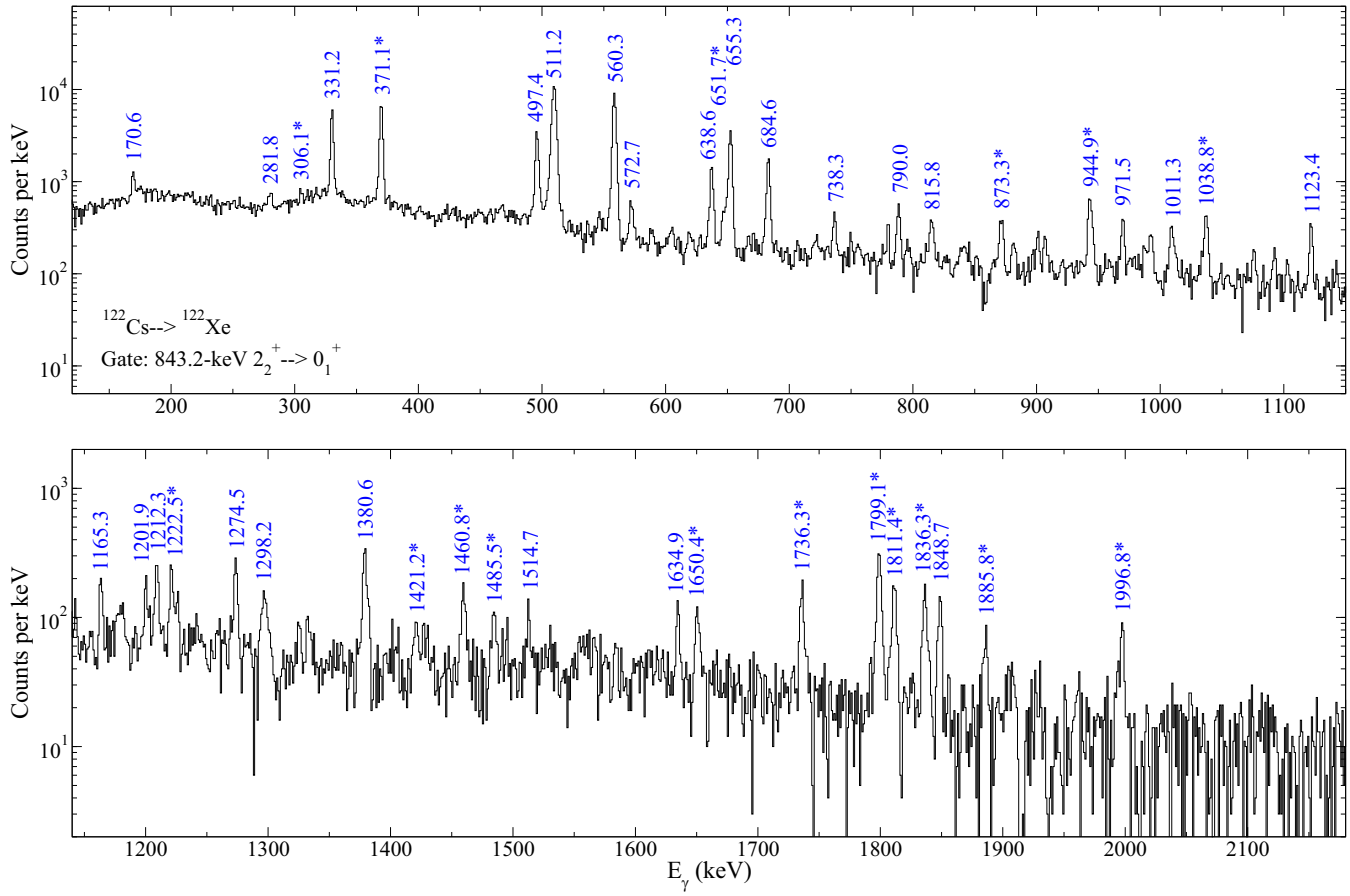

FIG. 4. Portion of the γ-ray spectrum observed from the long-cycle data with a coincidence condition placed on the 843.2 keV $2_2^+ \rightarrow 0_1^+$ γ ray. Some of the prominent γ rays observed are labeled with their energy in keV and the γ rays used for an angular correlation analysis with the 843.2 keV γ ray are indicated by an asterisk.

derived in this manner by the total intensity of all γ rays from the level of interest [39,40]. Labeling $I'_{\gamma_f} = N_c/\epsilon(\gamma_f)$, the branching ratio for any level was thus

$$\mathrm{BR}(\gamma_f) = \frac{\dfrac{I'_{\gamma_f}}{P_{\gamma_d}\epsilon(\gamma_d)}}{\sum_j \dfrac{I'_{\gamma_{fj}}}{P_{\gamma_{dj}}\epsilon(\gamma_{dj})}}, \tag{2}$$

where the summation over j extends to all transitions decaying from the level of interest. No correction for conversion electron emission was made since this cannot be determined for all transitions. The branching ratios for the levels populated by short and long decays of ^{122}Cs are displayed in Table I and Table II, respectively.

B. γ-ray intensities

Intensities of γ rays from levels populated by the short- and long-lived states of ^{122}Cs were calculated from the γ-ray singles data whenever possible. In order to separate the two decays, conditions on the clock time of the events following the beam implantation were placed on the long-cycle data to generate a spectrum containing (effectively) only the γ rays present from the decay of the $8^{(-)}$ isomer. The condition applied, $T > 150$ s following the cessation of the implantation, reduced the activity due to the 1^+ ^{122}Cs ground state to 1/132 of its value at end of the implant. Figure 5 displays the γ-ray singles spectrum generated in this manner, with the inset showing the effect of reduction of peaks from the short-lived decay. A spectrum consisting of γ rays from the short-lived ground-state decay is shown in Fig. 6. The singles spectra contain approximately 10^9 and 2.2×10^9 counts from short- and long-lived decays of ^{122}Cs, respectively. For well-resolved γ rays significantly above the background, the intensities were taken from the respective γ-ray singles spectrum. In many cases, however, only one γ ray decaying from a particular level could be observed sufficiently well resolved in the singles spectrum, and the intensity of the remaining decaying γ rays were deduced using the branching ratios, i.e.,

$$I_\gamma(B) = I_\gamma(A)\frac{\mathrm{BR}(B)}{\mathrm{BR}(A)}, \tag{3}$$

where $I_\gamma(A)$ represents the intensity determined from the singles spectrum. For cases where no γ rays from the level of interest were well resolved in the singles spectrum, the intensity scale of a second level was deduced by taking an intensity ratio in a coincidence spectrum to a known γ ray from a

TABLE I. Levels and observed γ rays in ^{122}Xe populated in the β^+/EC decay of ^{122}Cs 1^+ ground state. The intensity (I_γ) of each γ ray is given relative to that of the 331 keV $2_1^+ \rightarrow 0_1^+$ γ ray defined to be 10 000 units. The normalization factor for converting the relative to absolute β-feeding intensities is 0.009 05(16). The log ft values are lower limits on an absolute scale. All γ-ray energies include statistical uncertainties, and an additional systematic uncertainty of 0.2 keV has not been accounted for.

E_{initial} (keV)	j_i^π	E_γ (keV)	E_{final} (keV)	j_f^π	I_γ	ML	δ	BR	I_β	logft
331.26(9)	2^+	331.24(3)	0.0	0^+	10000	$E2$		100	26.2(10)	7.60(1)
828.61(10)	4^+	497.41(3)	331.26(9)	2^+	226(5)	$E2$		100	0.61(6)	9.06(3)
843.19(9)	2^+	511.21(3)	331.26(9)	2^+	<2107(65)	$M1, E2$		<84.3(4)	<16.6(7)	>7.62(2)
		843.16(4)	0.0	0^+	393(8)			>15.7(4)		
1149.31(11)	0^+	306.12(15)	843.19(9)	2^+	17.1(13)	$E2$		2.2(2)	7.37(16)	7.86(1)
		818.14(3)	331.26(9)	2^+	751.0(48)	$E2$		97.8(2)		
1214.28(10)	3^+	371.08(4)	843.19(9)	2^+	97.5(27)	$M1, E2$	$8.6^{+6.7}_{-2.7}$	30.7(7)	1.33(6)	8.57(2)
		385.69(6)	828.61(10)	4^+	26.1(9)	$M1, E2$	$2.8^{+0.5}_{-0.4}$	8.2(2)		
		883.00(3)	331.26(9)	2^+	194.2(42)	$M1, E2$	$0.05^{+0.04}_{-0.04}$	61.1(13)		
1402.82(12)	4^+	559.64(6)	843.19(9)	2^+	14.0(4)	$E2$		53.0(5)	0.057(17)	9.86(13)
		574.19(4)	828.61(10)	4^+	12.38(30)	$M1, E2$	$3.0^{+3.3}_{-1.3}$	47.0(5)		
1494.97(10)	2^+	345.7(1)	1149.31(11)	0^+	17.4(7)			4.8(1)	1.68(7)	8.36(2)
		651.71(5)	843.19(9)	2^+	27.2(12)	$M1, E2$	$0.8^{+0.6}_{-0.2}$	7.5(2)		
		666.41(4)	828.61(10)	4^+	53.2(18)	$E2$		14.6(4)		
		1163.71(4)	331.26(9)	2^+	93.1(20)	$M1, E2$	4^{+2}_{-1}	25.6(6)		
		1494.77(5)	0.0	0^+	173(5)			47.5(10)		
1716.49(12)	0^+	873.30(6)	843.19(9)	2^+	64.3(32)	$E2$		26.9(9)	2.06(7)	8.18(2)
		1385.23(4)	331.26(9)	2^+	174(4)	$E2$		73.1(9)		
1788.07(13)	0^+	944.91(5)	843.19(9)	2^+	76(7)	$E2$		77.2(13)	0.97(7)	8.48(4)
		1456.81(15)	331.26(9)	2^+	22.4(14)	$E2$		22.8(13)		
1817.88(12)	(3^-)	989.3(1)	828.61(10)	4^+	4.17(34)			7.1(5)	0.482(16)	8.77(2)
		1486.6(1)	331.26(9)	2^+	55.0(16)	$(E1)$	$-0.02^{+0.06}_{-0.06}$	92.9(5)		
1881.99(11)	2^+	387.0(2)	1494.97(10)	2^+	8.42(36)			5.67(16)	0.83(4)	8.51(2)
		667.70(5)	1214.28(10)	3^+	35.9(12)			24.17(57)		
		732.7(2)	1149.31(11)	0^+	1.69(18)			1.14(7)		
		1038.79(5)	843.19(9)	2^+	64.2(14)	$M1, E2$	0.4(1)	43.24(100)		
		1053.42(13)	828.61(10)	4^+	6.06(35)			4.08(14)		
		1550.7(1)	331.26(9)	2^+	26.2(10)	$M1, E2$	$-1.2^{+0.5}_{-0.4}$	17.67(46)		
		1882.0(2)	0.0	0^+	5.97(30)			4.03(13)		
1921.17(15)	$(4)^+$	706.3(2)	1214.28(10)	3^+	1.27(25)			10.4(13)	0.122(12)	9.32(5)
		1078.0(9)	843.19(9)	2^+	4.7(10)			38.7(40)		
		1589.91(13)	331.26(9)	2^+	6.2(6)			50.9(40)		
2012.07(11)	(1)	1680.81(14)	331.26(9)	2^+	3.86(45)			7.2(7)	0.260(34)	8.95(6)
		2012.1(2)	0.0	0^+	49.5(31)			92.8(7)		
2046.97(15)	2^+	1715.70(11)	331.26(9)	2^+	17.1(4)	$M1, E2$	$-1.6^{+0.5}_{-0.6}$	100	0.123(5)	9.26(2)
2065.67(10)	2^+	349.2(8)	1716.49(12)	0^+	29.9(55)			10.4(10)	2.66(8)	7.92(2)
		851.42(8)	1214.28(10)	3^+	24.9(17)			8.6(4)		
		1222.51(6)	843.19(9)	2^+	49.1(30)	$M1, E2$	-5^{+2}_{-8}	17.0(7)		
		1237.03(5)	828.61(10)	4^+	43.5(27)	$E2$		15.1(6)		
		1734.41(5)	331.26(9)	2^+	129.2(28)	$M1, E2$	$0.13^{+0.05}_{-0.05}$	44.7(14)		
		2065.7(2)	0.0	0^+	12.3(15)			4.2(3)		
2223.79(22)	0^+	1380.6(2)	843.19(9)	2^+	10.5(18)	$E2$		14.7(21)	0.714(25)	8.42(2)
		1891.83(8)	331.26(9)	2^+	60.9(17)	$E2$		85.3(21)		
2249.08(23)		1034.8(5)	1214.28(10)	3^+	0.33(7)			100	0.0033(7)	10.74(15)
2264.38(11)	2^+	446.5(1)	1817.88(12)	(3^-)	5.81(28)			3.29(13)	1.736(34)	8.02(2)
		476.3(3)	1788.07(13)	0^+	1.69(18)			0.96(8)		
		769.4(2)	1494.97(10)	2^+	5.15(43)			2.92(18)		
		1050.11(17)	1214.28(10)	3^+	4.52(16)			2.80(17)		
		1421.21(12)	843.19(9)	2^+	24.7(19)	$M1, E2$	$2.3^{+5.4}_{-1.3}$	14.01(79)		
		1435.81(13)	828.61(10)	4^+	7.6(4)			4.30(17)		
		1933.10(5)	331.26(9)	2^+	127(3)	$M1, E2$	$-0.9^{+0.3}_{-0.2}$	71.72(160)		
2284.98(23)		1070.71(12)	1214.28(10)	3^+	7.15(19)			100	0.0715(19)	9.39(2)
2303.97(12)	0^+	238.3(4)	2065.67(10)	2^+	4.4(5)			3.40(24)	1.28(4)	8.13(2)
		291.9(4)	2012.07(11)	(1)	1.11(18)			0.86(6)		

TABLE I. (*Continued.*)

E_{initial} (keV)	j_i^π	E_γ (keV)	E_{final} (keV)	j_f^π	I_γ	ML	δ	BR	I_β	logft
		422.0(2)	1881.99(11)	2^+	7.3(7)			5.65(34)		
		809.0(1)	1494.97(10)	2^+	23.1(12)			17.95(69)		
		1460.78(7)	843.19(9)	2^+	49.8(34)	$E2$		38.82(130)		
		1972.7(1)	331.26(9)	2^+	42.8(10)	$E2$		33.32(110)		
2328.66(15)	2^+	1485.52(6)	843.19(9)	2^+	0.91(8)	$M1, E2$	$-0.6^{+0.3}_{-0.5}$	93.1(5)	−0.013(2)	
		2328.6(2)	0.0	0^+	0.068(8)			6.9(5)		
2341.67(13)	$1,2^+$	2010.41(6)	331.26(9)	2^+	38.5(15)	$M1, E2$		72.6(6)	0.240(21)	8.83(5)
		2341.7(2)	0.0	0^+	14.49(37)			27.4(6)		
2406.76(22)	(1^+), 2^+, 3, (4^+)	2075.5(1)	331.26(9)	2^+	25.3(6)			100	0.253(6)	8.79(2)
2411.78(23)		1197.51(23)	1214.28(10)	3^+	2.86(14)			100	0.0286(14)	9.73(2)
2493.61(15)	0^+	998.6(2)	1494.97(10)	2^+	0.85(11)			3.2(3)	0.262(10)	8.73(2)
		1650.41(7)	843.19(9)	2^+	11.35(25)	$E2$		43.3(17)		
		2162.41(6)	331.26(9)	2^+	14.0(9)	$E2$		53.5(18)		
2501.98(23)		1287.7(2)	1214.28(10)	3^+	4.00(16)			100	0.0400(16)	9.54(2)
2511.27(17)	(1^+), 2^+	1668.1(3)	843.19(9)	2^+	1.36(31)			11.3(20)	0.12(3)	9.05(12)
		2180.0(1)	331.26(9)	2^+	9.6(30)	$M1, E2$		79.6(26)		
		2511.3(2)	0.0	0^+	1.10(36)			9.1(8)		
2530.35(11)	0^+	188.71(6)	2341.67(13)	$1,2^+$	29.0(14)			7.15(18)	4.09(6)	7.52(2)
		201.71(35)	2328.66(15)	2^+	1.74(18)			0.43(3)		
		266.0(9)	2264.38(11)	2^+	2.38(21)			0.59(3)		
		464.7(1)	2065.67(10)	2^+	16.3(11)			4.03(16)		
		518.3(2)	2012.07(11)	(1)	8.2(5)			2.02(8)		
		648.33(4)	1881.99(11)	2^+	65.7(37)			16.23(55)		
		1035.31(4)	1494.97(10)	2^+	136.7(29)			32.73(81)		
		2199.11(5)	331.26(9)	2^+	149.1(32)	$E2$		36.82(88)		
2552.26(22)	$(1, 2)^+$	2221.0(2)	331.26(9)	2^+	4.87(48)			60.4(34)	0.049(7)	9.43(7)
		2552.3(2)	0.0	0^+	3.20(56)			39.6(34)		
2579.49(22)	1^+	1736.3(1)	843.19(9)	2^+	18.2(14)	$M1, E2$	$-3.7^{+1.6}_{-4.0}$	93.3(5)	0.195(15)	8.81(4)
		2579.5(2)	0.0	0^+	1.31(14)			6.7(5)		
2596.95(14)	2^+	1194.1(3)	1402.82(12)	4^+	16.7(16)			40.25(16)	0.416(24)	8.47(3)
		1382.7(1)	1214.28(10)	3^+	0.44(7)			1.07(10)		
		1753.8(3)	843.19(9)	2^+	23.4(18)			56.18(18)		
		1768.3(2)	828.61(10)	4^+	0.151(33)			0.36(5)		
		2265.7(1)	331.26(9)	2^+	0.89(14)	$M1, E2$	$-0.5^{+0.3}_{-0.8}$	2.14(21)		
2618.96(22)		2287.7(2)	331.26(9)	2^+	6.20(23)			100	0.062(2)	9.30(2)
2642.25(10)	2^+	313.6(4)	2328.66(15)	2^+	0.49(8)			0.27(3)	1.80(3)	7.82(2)
		576.6(2)	2065.67(10)	2^+	1.83(20)			1.02(8)		
		630.2(2)	2012.07(11)	(1)	0.65(9)			0.36(4)		
		760.31(13)	1881.99(11)	2^+	6.4(7)			3.56(26)		
		824.4(4)	2046.97(15)	2^+	1.14(17)			0.63(7)		
		925.7(8)	1716.49(12)	0^+	0.81(13)			0.46(5)		
		1147.3(2)	1494.97(10)	2^+	4.47(52)			2.49(20)		
		1239.4(3)	1402.82(12)	4^+	2.62(23)			1.46(9)		
		1428.02(5)	1214.28(10)	3^+	29.2(15)			16.24(63)		
		1492.9(6)	1149.31(11)	0^+	0.44(8)			0.24(3)		
		1799.14(4)	843.19(9)	2^+	122.8(27)	$M1, E2$	−0.7(2)	68.34(8)		
		1813.6(3)	828.61(10)	4^+	2.80(23)			1.56(9)		
		2311.0(2)	331.26(9)	2^+	6.05(49)	$M1, E2$	$-1.2^{+0.6}_{-0.7}$	3.37(19)		
2654.61(12)	2^+	938.1(2)	1716.49(12)	0^+	0.89(11)			0.86(7)	1.035(21)	8.05(2)
		1251.8(3)	1402.82(12)	4^+	1.29(17)			1.24(11)		
		1440.3(1)	1214.28(10)	3^+	5.82(44)			5.63(28)		
		1505.3(5)	1149.31(11)	0^+	1.38(14)			1.33(8)		
		1811.41(5)	843.19(9)	2^+	60.2(13)	$M1, E2$	50(43)	58.18(92)		
		1826.0(1)	828.61(10)	4^+	5.39(38)			5.21(22)		
		2323.4(1)	331.26(9)	2^+	10.7(8)	$M1, E2$	$0.4^{+0.2}_{-0.1}$	10.38(46)		
		2654.6(2)	0.0	0^+	17.8(14)			17.17(75)		

TABLE I. (*Continued.*)

E_{initial} (keV)	j_i^π	E_γ (keV)	E_{final} (keV)	j_f^π	I_γ	ML	δ	BR	I_β	logft
2679.47(15)	2^+	1184.5(6)	1494.97(10)	2^+	0.83(11)			3.60(39)	0.230(17)	8.69(5)
		1836.32(6)	843.19(9)	2^+	21.4(17)	$M1, E2$	$-2.1^{+0.6}_{-0.9}$	92.99(69)		
		2348.2(1)	331.26(9)	2^+	0.78(16)	$M1, E2$	$-1.1^{+0.8}_{-0.5}$	3.41(58)		
2704.96(22)		2373.7(2)	331.26(9)	2^+	5.36(52)			100	0.054(5)	9.32(5)
2728.99(13)	2^+	1514.71(6)	1214.28(10)	3^+	35.6(15)			31.19(73)	1.141(28)	7.98(2)
		1579.7(5)	1149.31(11)	0^+	1.48(17)			1.30(9)		
		1885.8(1)	843.19(9)	2^+	29.9(21)	$M1, E2$	$-2.0^{+0.8}_{-1.8}$	26.21(92)		
		1900.41(25)	828.61(10)	4^+	3.22(28)			2.83(15)		
		2397.7(1)	331.26(9)	2^+	43.9(10)	$M1, E2$	0.04(8)	38.47(11)		
2746.90(17)	$1,2^+$	1597.6(8)	1149.31(11)	0^+	0.228(59)			7.8(15)	0.029(4)	9.56(7)
		1903.70(35)	843.19(9)	2^+	2.68(40)			92.2(15)		
2751.06(22)		1907.93(25)	843.19(9)	2^+	3.76(46)			69.2(27)	0.054(5)	9.29(5)
		2419.8(2)	331.26(9)	2^+	1.67(29)			30.8(27)		
2805.14(15)	$2^+, 3, 4^+$	987.3(5)	1817.88(12)	(3^-)	1.00(12)			2.17(24)	0.459(10)	8.33(2)
		1590.9(4)	1214.28(10)	3^+	3.82(34)			8.32(67)		
		2473.91(7)	331.26(9)	2^+	41.1(9)			89.51(69)		
2840.00(13)	0^+	827.9(1)	2012.07(11)	(1)	15.5(12)			24.9(13)	0.621(16)	8.188(2)
		1996.82(6)	843.19(9)	2^+	40.9(9)	$E2$		65.8(19)		
		2508.83(16)	331.26(9)	2^+	5.8(7)			9.3(8)		
2855.86(22)		2524.61(24)	331.26(9)	2^+	4.70(23)			100	0.047(2)	9.30(3)
2894.78(14)	$1^+, 2^+$	1178.3(6)	1716.49(12)	0^+	1.40(23)			8.6(6)	0.162(12)	8.73(4)
		1399.8(8)	1494.97(10)	2^+	3.07(50)			18.9(13)		
		1680.51(14)	1214.28(10)	3^+	8.1(11)			49.8(21)		
		2563.5(2)	331.26(9)	2^+	3.68(20)			22.7(16)		
2919.97(17)		2588.7(2)	331.26(9)	2^+	3.12(19)			100	0.0312(19)	9.44(4)
2921.27(17)		1426.3(7)	1494.97(10)	2^+	7.2(8)			100	0.072(8)	9.08(5)
2931.86(22)	2^+	2600.6(1)	331.26(9)	2^+	19.8(8)	$M1, E2$	$-2.0^{+0.5}_{-0.7}$	33.6(11)	0.588(25)	8.16(2)
		2931.9(2)	0.0	0^+	39.0(24)			66.4(11)		
2951.72(15)	$1^+, 2^+$	1737.5(4)	1214.28(10)	3^+	0.66(16)			18.4(20)	0.036(4)	9.36(6)
		1802.4(3)	1149.31(11)	0^+	0.92(22)			25.6(27)		
		2108.5(4)	843.19(9)	2^+	2.02(31)			56.0(33)		
2974.36(22)		2643.1(2)	331.26(9)	2^+	7.66(25)			100	0.077(3)	9.02(2)
2989.07(25)		942.1(6)	2046.97(15)	2^+	2.21(13)			100	0.0221(13)	9.55(3)
2996.06(22)	0^+	2664.8(2)	331.26(9)	2^+	4.63(22)	$E2$		100	0.046(2)	9.23(3)
3009.48(13)	$(1),2^+$	962.5(4)	2046.97(15)	2^+	0.94(14)			2.24(18)	0.420(12)	8.26(2)
		997.4(2)	2012.07(11)	(1)	1.13(17)			2.68(22)		
		1514.5(9)	1494.97(10)	2^+	2.69(35)			6.41(46)		
		1860.2(1)	1149.31(11)	0^+	8.0(5)			19.09(69)		
		2678.2(1)	331.26(9)	2^+	14.8(4)	$M1, E2$		35.23(11)		
		3009.5(2)	0.0	0^+	14.4(9)			34.35(11)		
3042.26(22)		2711.0(2)	331.26(9)	2^+	5.53(25)			100	0.0553(25)	9.13(2)
3064.48(22)		2733.2(5)	331.26(9)	2^+	3.64(34)			100	0.0364(34)	9.30(5)
3078.37(14)	$1,2^+$	1031.4(4)	2046.97(15)	2^+	0.47(10)			2.5(3)	0.186(10)	9.58(3)
		1066.3(4)	2012.07(11)	(1)	0.78(15)			4.2(5)		
		1583.4(3)	1494.97(10)	2^+	3.78(49)			20.3(14)		
		2747.11(15)	331.26(9)	2^+	6.94(25)			37.2(20)		
		3078.4(2)	0.0	0^+	6.68(79)			35.8(19)		
3089.96(22)		2758.7(2)	331.26(9)	2^+	6.50(25)			100	0.0650(25)	9.03(2)
3104.26(22)	2^+	2773.00(15)	331.26(9)	2^+	18.76(47)	$M1, E2$	$-1.3(5)$	100	0.1876(47)	8.56(2)
3119.89(22)	$1,2^+$	2276.7(3)	843.19(9)	2^+	1.41(24)			17.3(33)	0.82(20)	8.92(11)
		3119.9(2)	0.0	0^+	6.7(19)			82.7(33)		
3130.56(22)	0^+	2799.30(14)	331.26(9)	2^+	10.32(32)	$E2$		100	0.1032(32)	8.81(2)
3170.66(22)		2839.43(15)	331.26(9)	2^+	17.89(44)			100	0.1789(44)	8.55(2)
3196.46(22)		2865.21(35)	331.26(9)	2^+	5.46(38)			100	0.0546(38)	9.05(4)
3245.36(22)		2914.11(16)	331.26(9)	2^+	12.54(35)			100	0.1254(35)	8.66(2)
3258.48(22)		2927.2(2)	331.26(9)	2^+	9.21(32)			100	0.0921(32)	8.79(2)
3293.06(22)		2961.8(1)	331.26(9)	2^+	26.0(6)			72.0(8)	0.362(8)	8.18(2)

TABLE I. (*Continued.*)

E_{initial} (keV)	j_i^π	E_γ (keV)	E_{final} (keV)	j_f^π	I_γ	ML	δ	BR	I_β	logft
		3293.1(2)	0.0	0^+	10.1(5)			28.0(8)		
3418.56(22)		3087.2(5)	331.26(9)	2^+	4.50(58)			100	0.045(6)	9.01(6)
3421.67(15)		1603.8(2)	1817.88(12)	(3^-)	4.16(23)			28.1(22)	0.148(12)	8.50(4)
		2207.4(2)	1214.28(10)	3^+	6.6(9)			44.7(28)		
		3090.4(5)	331.26(9)	2^+	4.02(77)			27.2(27)		
3430.56(22)		3099.3(3)	331.26(9)	2^+	3.26(26)			100	0.033(3)	9.15(4)
3456.36(22)	0^+	3125.1(2)	331.26(9)	2^+	1.42(49)	$E2$		100	0.014(5)	9.48(14)
3525.66(22)		3194.4(2)	331.26(9)	2^+	2.44(68)			100	0.024(7)	9.22(12)
3528.98(23)		2314.7(3)	1214.28(10)	3^+	4.07(21)			100	0.0407(21)	8.99(3)
3724.18(23)		2509.9(5)	1214.28(10)	3^+	8.79(29)			100	0.0879(29)	8.54(2)
3874.08(23)		2659.8(7)	1214.28(10)	3^+	2.04(24)			100	0.0204(24)	9.10(6)

reference level for which singles intensities were available via

$$I_\gamma(B) = I_\gamma(A)\frac{I_{\text{coinc}}(B)}{I_{\text{coinc}}(A)}. \tag{4}$$

The intensities determined are given in Tables I and II for the short-lived and long-lived decays, respectively.

C. β intensity and log ft value

The intensity of the β feeding to an excited state was calculated as the difference of the γ-ray intensities of feeding and draining transitions and any excess intensity of draining γ rays was attributed to β feeding intensity. Normalization factors relative to absolute intensities are given in a caption of the Tables I and II. log ft values were calculated using analysis program LOGFT [41]. The intensity of β feeding to levels populated by short and long decays of ^{122}Cs along with the absolute log ft values are displayed in Tables I and II. For the decay of the ^{122}Cs 1^+ state, it was assumed that the β^+/EC intensity to the ^{122}Xe ground state was 48(3)% [17]. Since the Q value for the decay is large, $Q = 7220(30)$ keV, it is expected that there remain many γ rays unobserved from the decay of high-lying levels (note that the highest energy level observed in the present work was at 4813.6 keV, approximately 2.4 MeV below the maximum energy allowed by the Q value), such that the I_β values should be considered as upper limits and hence the log ft value as lower limits.

D. γ-γ angular correlations

The angular correlation of two γ rays emitted in a coincidence cascade depends on the spins of levels involved and the multipolarities and mixing ratios of the transitions in cascade. The angular correlation of the γ ray associated with the transition $J_2 \to J_3$ with respect to the direction of the γ ray associated with the transition $J_1 \to J_2$ is

$$W(\theta) = \sum_{k=0}^{\infty} a_k P_k(\cos\theta), \tag{5}$$

where a_k is a coefficient dependent on spins of states involved and the multipolarities of the γ rays, and $P_k(\cos\theta)$ are Legendre polynomials. The assumption made is that the initial state is randomly orientated and then decays by emission of a sequence of two or more γ rays.

Since no direction in space is preferred for the state J_1, and in the most common cases only two multipoles contribute to the transition, the a_k coefficients are expressed as given in Ref. [42]:

$$a_k = Q_k B_k(J_2) R_k(J_2 J_3), \tag{6}$$

where Q_k are attenuation coefficients related to the detector size and are adopted from Ref. [43], $B_k(J_2)$ depends on the nuclear alignment only, and $R_k(J_2J_3)$ depends on quantities which characterize the transition. In the present analysis, the $B_k(J_2)$ and $R_k(J_2J_3)$ coefficients were adopted from Ref. [42]. The probability is restricted to even values of k due to the required symmetry about 90°, and the series is terminated at a maximum value of $k = 4$ since multipolarities above $E2$ were not considered. The numbers of expected detector pairs for the 8π spectrometer were 30, 60, 60, 30, and 10 detector pairs for the five opening angles, as measured to the center of the HPGe detectors, of 41.8°, 70.5°, 109.5°, 138.2°, and 180°, respectively. However, in the analysis of the angular correlations, data from three HPGe detectors were not included in order to maintain the highest overall quality. For the 17 detectors remaining, the number of detector pairs were reduced to 21, 45, 42, 21, and 7, respectively.

In all cases, the $J_2 \to J_3$ transition was chosen to assure a pure $E2$ multipolarity with J_2 and J_3 known. Thus, the angular correlation depends on only the spin of the initial level, J_1, and the mixing ratio δ of the $J_1 \to J_2$ transition. The spin J_1 was generally excluded if the χ^2 value of the fit to the experimental data exceeded the 95% level of the cumulative probability distribution, i.e., there is less than a 5% chance of statistical fluctuations yielding a χ^2 value greater than this. However, constraints on J_1 values arising from other γ-ray transition branches that would require, for example, unreasonable transition multipolarities were also taken into account. In some cases, we strongly favor a particular spin even if several solutions have a χ^2 value below the 95% limit, usually based on level systematics or if it is an apparent member of a rotational band.

The transition mixing ratio δ was extracted as the value corresponding to the minimum χ^2 value, with the

TABLE II. Levels and observed γ ray in ^{122}Xe populated in the β^+/EC decay of ^{122}Cs $8^{(-)}$ isomeric state. The intensity (I_γ) of each γ ray is given relative to that of the 331 keV $2_1^+ \rightarrow 0_1^+$ γ ray defined to be 10 000 units. The normalization factor for converting the relative to absolute β-feeding intensities is 0.009 46(18). The logft values are lower limits on an absolute scale. All γ-ray energies include statistical uncertainties, and an additional systematic uncertainty of 0.2 keV has not been accounted for.

E_{initial} (keV)	j_i^π	E_γ (keV)	E_{final} (keV)	j_f^π	I_γ	ML	δ	BR	I_β	logft
331.18(9)	2^+	331.24(3)	0.0	0^+	10000	$E2$		100	−2.1(27)	
828.62(11)	4^+	497.37(3)	331.18(9)	2^+	8084(173)	$E2$		100	0.90(217)	
843.21(10)	2^+	511.87(3)	331.18(9)	2^+	<1355(52)	$M1, E2$		<83.67(44)	<5.53(55)	>9.15(14)
		843.21(4)	0.0	0^+	264(6)			>16.33(44)		
1214.30(11)	3^+	371.11(4)	843.21(10)	2^+	323(8)	$M1, E2$	$0.06^{+0.03}_{-0.02}$	30.8(64)	0.85(37)	
		385.68(6)	828.62(11)	4^+	82.6(21)	$M1, E2$	$4.3^{+1.2}_{-0.8}$	7.9(1)		
		883.03(3)	331.18(9)	2^+	644(14)	$M1, E2$	$0.06^{+0.03}_{-0.01}$	61.3(12)		
1402.83(12)	4^+	559.58(3)	843.21(10)	2^+	657(15)	$E2$		52.9(2)	0.69(30)	
		574.23(3)	828.62(11)	4^+	585(13)	$M1, E2$	$3.0^{+10.7}_{-4.4}$	47.1(2)		
1467.23(12)	6^+	638.61(3)	828.62(11)	4^+	6141(130)	$E2$		100	4.8(14)	8.97(14)
1774.62(12)	5^+	307.4(3)	1467.23(12)	6^+	142(6)			10.01(10)	1.26(61)	
		371.82(11)	1402.83(12)	4^+	125(5)			8.75(10)		
		560.33(3)	1214.30(11)	3^+	824(32)	$E2$		57.85(25)		
		946.02(4)	828.62(11)	4^+	333(12)	$M1, E2$	$0.39^{+0.09}_{-0.07}$	23.39(21)		
1817.89(16)	(3^-)	1486.64(14)	331.18(9)	2^+	39.9(16)	$(E1)$	$4.5^{+0.8}_{-0.5}$	100	0.370(16)	9.95(13)
1854.50(13)	4^+	1011.31(11)	843.21(10)	2^+	60.3(58)			32.0(16)	0.98(9)	9.51(14)
		1025.43(16)	828.62(11)	4^+	86.4(47)	$M1, E2$	$-3.7^{+1.3}_{-5.0}$	45.8(16)		
		1523.3(1)	331.18(9)	2^+	41.9(10)			22.2(8)		
1920.59(13)	(4^+)	706.32(16)	1214.30(11)	3^+	10.9(15)			13.1(13)	0.20(5)	10.18(17)
		1078.01(16)	843.21(10)	2^+	25.6(28)			30.6(21)		
		1589.88(7)	331.18(9)	2^+	47.1(11)			56.3(24)		
2056.80(12)	6^+	589.60(4)	1467.23(12)	6^+	258(6)	$M1, E2$	$-0.01^{+0.06}_{-0.05}$	24.4(3)	4.31(24)	8.78(14)
		654.03(3)	1402.83(12)	4^+	763(21)	$E2$		71.9(3)		
		1228.2(3)	828.62(11)	4^+	39.4(27)			3.7(2)		
2126.84(13)	(5^-)	659.6(2)	1467.23(12)	6^+	14.9(11)			3.62(23)	2.64(14)	8.96(13)
		724.0(3)	1402.83(12)	4^+	17.6(11)			4.28(23)		
		1298.23(4)	828.62(11)	4^+	378(13)	$(E1)$	0.01(5)	92.10(30)		
2158.50(23)		944.1(9)	1214.30(11)	3^+	4.9(25)			100	0.049(26)	10.7(3)
2162.52(15)	(4^-)	948.2(3)	1214.30(11)	3^+	20.6(5)			15.0(11)	0.527(19)	9.65(13)
		1333.90(7)	828.62(11)	4^+	60.8(14)	$(E1)$	−1.0(4)	85.0(11)		
2217.82(12)	8^+	750.61(3)	1467.23(12)	6^+	1090(23)	$E2$		100	0.60(28)	9.56(18)
2379.61(13)	(5^+)	459.0(6)	1920.59(13)	(4^+)	9.4(13)			4.1(2)	1.54(15)	9.08(14)
		525.11(25)	1854.50(13)	4^+	25.1(37)			10.9(7)		
		605.0(2)	1774.62(12)	5^+	34.0(47)			14.8(9)		
		976.81(15)	1402.83(12)	4^+	51.9(56)			22.6(8)		
		1165.31(7)	1214.30(11)	3^+	109(10)			47.6(11)		
2401.37(13)	(6^+)	480.8(5)	1920.59(13)	(4^+)	6.4(6)			5.2(4)	0.44(5)	9.61(14)
		546.91(16)	1854.50(13)	4^+	30.7(30)			24.6(15)		
		1572.92(6)	828.62(11)	4^+	87.5(34)			70.2(16)		
2452.23(23)		985.0(3)	1467.23(12)	6^+	10.9(14)			100	0.109(14)	10.21(14)
2459.22(12)	7^+	402.4(2)	2056.80(13)	6^+	19.0(15)			2.6(1)	1.84(42)	8.98(17)
		684.60(3)	1774.62(12)	5^+	651(40)	$E2$		89.4(18)		
		992.0(1)	1467.23(12)	6^+	58.2(26)			8.0(34)		
2496.11(13)	5^-	1093.3(1)	1402.83(12)	4^+	51.6(11)	$E1$		50.0(11)	0.56(3)	9.47(14)
		1667.5(1)	828.62(11)	4^+	51.7(25)	$E1$	−0.02(11)	50.0(11)		
2526.21(12)	(6^+)	469.4(1)	2056.80(12)	6^+	25.5(11)			6.1(1)	0.77(13)	9.31(15)
		605.64(7)	1920.59(13)	(4^+)	48.2(33)			11.6(3)		
		672.73(14)	1854.50(13)	4^+	35.2(32)			8.4(3)		
		751.62(5)	1774.62(12)	5^+	51.0(28)			12.2(3)		
		1059.02(5)	1467.23(12)	6^+	79.6(29)	$M1, E2$	0.2(2)	19.1(3)		
		1123.44(5)	1402.83(12)	4^+	87.4(32)			20.9(3)		
		1697.64(5)	828.62(11)	4^+	90.7(20)	$(E2)$		21.7(3)		
2556.23(12)	(6^-)	393.7(1)	2162.52(15)	(4^-)	19.3(11)			4.2(1)	0.98(15)	9.19(15)

TABLE II. (*Continued.*)

E_{initial} (keV)	j_i^π	E_γ (keV)	E_{final} (keV)	j_f^π	I_γ	ML	δ	BR	I_β	logft
		429.4(1)	2126.84(13)	(5^-)	35.5(15)			7.6(2)		
		781.63(4)	1774.62(12)	5^+	119(26)			25.6(5)		
		1089.04(3)	1467.23(12)	6^+	291(11)	$(E1)$	$-0.7^{+0.3}_{-0.2}$	62.6(5)		
2565.28(12)	(7^-)	438.4(1)	2126.84(13)	(5^-)	34.3(14)			3.26(11)	1.62(28)	8.97(14)
		1098.04(3)	1467.23(12)	6^+	1016(22)	$(E1)$	$-0.03^{+0.05}_{-0.04}$	96.74(11)		
2595.09(16)	$(4^+, 5^-)$	432.73(26)	2162.52(15)	(4^-)	9.50(65)			9.4(5)	0.883(36)	9.22(13)
		777.2(2)	1817.89(16)	(3^-)	2.89(31)			2.9(3)		
		1766.51(14)	828.62(11)	4^+	88.7(35)			87.7(18)		
2604.52(16)	$4^+, 5, 6^+$	1201.9(1)	1402.83(12)	4^+	47.3(11)			100	0.333(14)	9.64(13)
2640.22(23)		1811.64(24)	828.62(11)	4^+	17.4(13)			100	0.174(13)	9.91(14)
2677.32(13)	(5,6)	620.5(2)	2056.80(12)	6^+	8.3(7)			7.0(3)	0.58(5)	9.36(14)
		1210.1(1)	1467.23(12)	6^+	42.3(24)			35.7(8)		
		1274.5(1)	1402.83(12)	4^+	29.6(17)			25.0(7)		
		1848.7(1)	828.62(11)	4^+	38.3(8)			32.3(8)		
2696.76(13)	(6^-)	140.5(1)	2556.23(12)	(6^-)	22.8(13)			12.9(4)	0.39(9)	9.53(16)
		170.62(4)	2526.21(12)	(6^+)	108(7)			60.9(1)		
		200.71(25)	2496.11(13)	5^-	3.99(38)			2.3(1)		
		922.1(1)	1774.62(12)	5^+	42.4(10)			23.9(9)		
2715.40(23)		1247.9(1)	1467.23(12)	6^+	30.41(79)			100	0.304(8)	9.63(13)
2769.18(13)	$(5,6,7^+)$	212.9(3)	2556.23(12)	(6^-)	4.68(55)			2.9(3)	0.95(26)	9.10(18)
		994.58(5)	1774.62(12)	5^+	155(25)			97.1(3)		
2795.30(14)	8^+	577.2(2)	2217.82(12)	8^+	15.1(8)			14.8(6)	0.669(28)	9.25(13)
		738.32(5)	2056.80(12)	6^+	87.1(19)	$E2$		85.2(6)		
2812.03(23)		1344.8(1)	1467.23(12)	6^+	35.3(8)			100	0.353(8)	9.51(13)
2847.12(12)	(7^-)	281.8(1)	2565.28(12)	(7^-)	63.9(23)			11.40(29)	3.14(16)	8.55(14)
		351.0(2)	2496.11(13)	5^-	5.79(60)			1.03(7)		
		629.3(1)	2217.82(12)	8^+	9.1(10)			1.62(12)		
		790.03(5)	2056.80(12)	6^+	109(4)			19.52(30)		
		1379.93(4)	1467.23(12)	6^+	372(10)			66.43(36)		
2873.18(13)	(7^-)	176.44(5)	2696.76(13)	(6^-)	29.5(24)			2.67(18)	8.18(28)	8.12(13)
		307.91(5)	2565.28(12)	(7^-)	158(48)			14.20(18)		
		377.1(3)	2496.11(13)	5^-	11.7(9)			1.05(6)		
		471.8(4)	2401.37(13)	(6^+)	9.6(7)			0.86(5)		
		655.3(6)	2217.82(12)	8^+	11.6(8)			1.04(5)		
		1405.94(3)	1467.23(12)	6^+	890(23)			80.18(26)		
2879.12(18)	$(5,6,7^+)$	1104.5(1)	1774.62(12)	5^+	31.2(19)			52.0(14)	0.599(20)	9.26(13)
		1411.9(1)	1467.23(12)	6^+	28.8(7)			48.0(14)		
2926.47(13)	(7^-)	229.74(16)	2696.76(13)	(6^-)	11.3(11)			1.92(15)	4.31(14)	8.37(13)
		361.24(6)	2565.28(12)	(7^-)	101(32)			17.23(24)		
		525.1(3)	2401.37(13)	(6^+)	12.0(8)			2.04(10)		
		799.6(2)	2126.84(13)	(5^-)	27.4(12)			4.66(13)		
		1459.31(4)	1467.23(12)	6^+	436(12)			74.15(31)		
2929.62(16)	5,6,7	252.32(17)	2677.32(13)	(5,6)	15.7(21)			34.8(15)	0.45(3)	9.34(14)
		373.4(2)	2556.23(12)	(6^-)	8.2(7)			18.3(10)		
		872.8(1)	2056.80(12)	6^+	21.1(24)			46.9(15)		
2935.63(20)		1468.4(1)	1467.23(12)	6^+	23.5(6)			100	0.195(9)	9.71(14)
2942.92(23)		725.1(4)	2217.82(13)	8^+	17.0(11)			100	0.170(11)	9.77(14)
2955.52(13)	(7^+)	429.3(2)	2526.21(12)	(6^+)	17.4(28)			17.4(10)	0.64(10)	9.18(15)
		575.94(8)	2379.61(13)	(5^+)	52(74)			51.7(13)		
		737.7(8)	2217.82(12)	8^+	2.75(71)			2.7(4)		
		898.7(2)	2056.80(12)	6^+	16.5(23)			16.5(7)		
		1488.3(2)	1467.23(12)	6^+	11.7(11)			11.7(7)		
2963.52(13)	$(6^+, 7^-)$	368.4(2)	2595.09(16)	$(4^+, 5^-)$	12.8(7)			2.90(11)	3.74(12)	8.42(13)
		398.2(1)	2565.28(12)	(7^-)	41.3(18)			9.35(16)		
		407.3(1)	2556.23(12)	(6^-)	41.9(10)			9.49(19)		
		562.1(2)	2401.37(13)	(6^+)	10.12(74)			2.29(11)		

TABLE II. (*Continued.*)

E_{initial} (keV)	j_i^π	E_γ (keV)	E_{final} (keV)	j_f^π	I_γ	ML	δ	BR	I_β	logft
		836.7(1)	2126.84(13)	(5^-)	49.9(21)			11.30(20)		
		1496.31(4)	1467.23(12)	6^+	276(11)	$(M1, E2)$	$1.1^{+0.4}_{-0.2}$	62.59(35)		
		2134.9(3)	828.62(11)	4^+	9.2(9)			2.08(14)		
3002.32(14)	$(6)^+$	601.0(2)	2401.37(13)	(6^+)	13.3(11)			9.43(37)	0.50(10)	9.26(16)
		784.5(1)	2217.82(12)	8^+	30.2(19)			21.40(59)		
		1227.72(12)	1774.62(12)	5^+	56.5(42)			40.08(91)		
		1535.1(2)	1467.23(12)	6^+	41.0(17)			29.09(78)		
3008.75(13)	(8^-)	82.3(1)	2926.47(13)	(7^-)	17.1(29)			7.09(17)	1.26(22)	8.89(13)
		135.62(5)	2873.18(13)	(7^-)	82(14)			34.16(65)		
		161.6(1)	2847.12(12)	(7^-)	16.0(27)			6.62(18)		
		312.0(1)	2696.76(13)	(6^-)	13.7(26)			5.67(24)		
		443.50(13)	2565.28(12)	(7^-)	20.9(36)			8.68(30)		
		452.53(8)	2556.23(12)	(6^-)	53.0(89)			21.97(47)		
		549.53(15)	2459.22(12)	7^+	5.6(11)			2.31(12)		
		790.93(6)	2217.82(12)	8^+	32.5(39)			13.50(69)		
3017.51(23)		1242.9(1)	1774.62(12)	5^+	3.80(28)			100	0.038(3)	10.38(14)
3028.42(13)	$(6^+,7)$	423.9(2)	2604.52(16)	$4^+, 5, 6^+$	9.3(7)			2.73(11)	2.78(8)	8.51(13)
		472.05(14)	2556.23(12)	(6^-)	38.0(19)			11.18(32)		
		810.52(7)	2217.82(12)	8^+	56.5(26)			16.63(44)		
		971.51(4)	2056.80(12)	6^+	136.8(54)			40.26(91)		
		1561.11(6)	1467.23(12)	6^+	99.2(30)			29.20(69)		
3031.91(14)	(8^-)	236.6(8)	2795.30(14)	8^+	3.52(27)			0.79(3)	4.25(14)	8.32(13)
		466.6(1)	2565.28(12)	(7^-)	88.8(49)			19.87(24)		
		475.7(1)	2556.23(12)	(6^-)	54.3(24)			12.14(20)		
		572.73(5)	2459.22(12)	7^+	83.2(46)			18.63(24)		
		814.11(4)	2217.82(12)	8^+	217(12)			48.57(34)		
3033.60(23)	$(9)^-$	815.8(2)	2217.82(12)	8^+	235(5)			100	2.349(50)	8.58(13)
3039.92(23)	10^+	822.13(15)	2217.82(12)	8^+	32.7(8)	$E2$		100	0.327(8)	9.43(13)
3041.18(16)		984.4(2)	2056.80(12)	6^+	22.1(38)			34.2(17)	0.65(7)	9.14(14)
		1266.6(1)	1774.62(12)	5^+	32.8(60)			50.8(20)		
		1573.9(4)	1467.23(12)	6^+	9.7(12)			15.0(13)		
3070.01(13)	$5^+, 6, 7^+$	392.7(7)	2677.32(13)	(5,6)	8.5(11)			5.97(34)	0.57(8)	9.17(15)
		610.8(3)	2459.22(12)	7^+	10.2(11)			7.17(33)		
		690.4(2)	2379.61(13)	(5^+)	23.8(25)			16.67(74)		
		1013.1(1)	2056.80(12)	6^+	30.2(28)			21.16(68)		
		1295.4(1)	1774.62(12)	5^+	45.6(52)			31.93(98)		
		1602.8(1)	1467.23(12)	6^+	24.4(15)			17.10(64)		
3072.31(23)		1297.7(1)	1774.62(12)	5^+	16.7(7)			100	−0.175(13)	
3100.33(23)		544.1(2)	2556.23(12)	(6^-)	5.64(32)			100	0.056(3)	10.17(14)
3101.70(17)		1327.1(1)	1774.62(12)	5^+	4.64(31)			100	−0.012(7)	
3150.01(23)		1375.4(2)	1774.62(12)	5^+	2.48(22)			100	0.025(2)	10.50(14)
3152.37(15)	$7,8^+, 9^-$	225.9(1)	2926.47(13)	(7^-)	136(6)			41.5(5)	3.07(9)	8.40(13)
		279.23(8)	2873.18(13)	(7^-)	152(7)			46.4(5)		
		934.5(1)	2217.82(12)	8^+	39.5(9)			12.1(3)		
3175.09(18)		773.7(8)	2401.37(13)	(6^+)	7.0(11)			25.2(23)	0.28(6)	9.44(16)
		957.3(2)	2217.82(12)	8^+	20.7(19)			74.8(23)		
3178.51(15)		409.3(2)	2769.18(13)	$(5,6,7^+)$	2.98(38)			7.53(64)	0.396(44)	9.27(14)
		960.7(2)	2217.82(12)	8^+	5.42(77)			13.67(13)		
		1121.7(2)	2056.80(12)	6^+	3.69(54)			9.33(92)		
		1711.3(1)	1467.23(12)	6^+	27.5(14)			69.47(165)		
3182.22(23)		386.9(6)	2795.30(14)	8^+	7.65(84)			5.1(2)	0.92(7)	8.91(14)
		616.9(1)	2565.28(12)	(7^-)	9.12(24)			37.9(7)		
		723.0(7)	2459.22(12)	7^+	69.4(65)			45.3(7)		
		964.41(12)	2217.82(12)	8^+	18.0(13)			11.7(4)		
3191.40(15)	(8^-)	264.9(3)	2926.47(13)	(7^-)	4.23(31)			10.6(5)	0.121(21)	9.76(15)
		318.23(5)	2873.18(13)	(7^-)	26.29(58)			66.0(9)		

TABLE II. (*Continued.*)

E_{initial} (keV)	j_i^π	E_γ (keV)	E_{final} (keV)	j_f^π	I_γ	ML	δ	BR	I_β	logft
		732.2(1)	2459.22(12)	7^+	9.32(49)			23.4(8)		
3216.62(20)	(9^+)	281.0(2)	2935.63(20)		4.03(63)			13.6(16)	0.297(20)	9.38(14)
		757.4(1)	2459.22(12)	7^+	25.6(19)			86.4(16)		
3229.38(19)		356.2(3)	2873.18(13)	(7^-)	4.22(17)			100	−0.003(6)	
3232.33(23)		776.1(2)	2556.23(12)	(6^-)	8.22(35)			100	0.082(4)	9.93(14)
3234.51(13)	(8^+)	708.3(1)	2526.21(12)	(6^+)	38.7(37)			36.8(10)	0.095(87)	
		775.3(2)	2459.22(12)	7^+	9.9(9)			9.4(4)		
		1016.7(2)	2217.82(12)	8^+	10.4(10)			9.8(4)		
		1177.70(14)	2056.80(12)	6^+	19.5(17)			18.5(7)		
		1767.30(14)	1467.23(12)	6^+	26.8(14)			25.5(8)		
3240.46(16)		276.9(7)	2963.53(13)	$(6^+, 7^-)$	11.4(10)			22.1(13)	0.462(23)	9.17(14)
		1773.2(1)	1467.23(12)	6^+	40.0(18)			77.9(13)		
3243.02(23)	$(9)^-$	1025.2(1)	2217.82(12)	8^+	2.88(8)			100	0.0288(8)	10.38(14)
3256.93(15)		409.8(2)	2847.12(12)	(7^-)	6.1(9)			4.87(50)	1.04(7)	8.81(14)
		487.1(1)	2769.18(13)	$(5,6,7^+)$	26.9(23)			21.57(82)		
		797.10(5)	2459.22(12)	7^+	91.6(62)			73.56(94)		
3269.83(23)		1802.90(13)	1467.23(12)	6^+	12.5(16)			100	0.125(16)	9.73(15)
3284.83(23)		721.9(8)	2565.28(12)	(7^-)	2.22(46)			19.9(31)	0.112(8)	9.77(14)
		728.6(2)	2556.23(12)	(6^-)	8.97(68)			80.1(31)		
3287.04(15)		278.30(6)	3008.75(13)	(8^-)	115(12)			64.3(12)	1.64(13)	8.60(14)
		517.90(13)	2769.18(13)	$(5,6,7^+)$	13.9(16)			7.8(4)		
		827.8(1)	2459.22(12)	7^+	49.9(41)			27.9(11)		
3301.42(15)		454.3(2)	2847.12(12)	(7^-)	22.5(32)			59.7(26)	0.141(41)	9.67(22)
		1834.0(2)	1467.23(12)	6^+	15.2(14)			40.3(26)		
3305.42(15)		846.2(1)	2459.22(12)	7^+	27.5(46)			30.7(14)	0.70(11)	9.00(15)
		1530.8(1)	1774.62(12)	5^+	51.5(91)			57.4(16)		
		1838.2(2)	1467.23(12)	6^+	10.7(12)			11.9(10)		
3336.61(19)		541.3(2)	2795.30(14)	8^+	7.28(63)			11.6(7)	0.625(29)	8.99(14)
		1118.8(1)	2217.82(12)	8^+	55.3(28)			88.4(7)		
3343.33(23)		1876.10(15)	1467.23(12)	6^+	13.5(11)			100	0.135(11)	9.65(14)
3380.73(23)		1913.5(1)	1467.23(12)	6^+	18.7(12)			100	0.187(12)	9.48(14)
3388.32(18)		929.1(2)	2459.22(12)	7^+	15.36(45)			45.3(36)	0.339(28)	9.23(14)
		1170.50(15)	2217.82(12)	8^+	18.6(27)			54.7(36)		
3396.32(18)		937.1(3)	2459.22(12)	7^+	3.9(8)			27.1(35)	0.142(13)	9.62(14)
		1929.1(2)	1467.23(12)	6^+	10.2(10)			72.9(35)		
3424.81(14)		461.3(5)	2963.53(13)	$(6^+, 7^-)$	4.1(10)			7.17(60)	0.566(47)	8.98(14)
		859.5(3)	2565.28(12)	(7^-)	9.2(17)			16.30(72)		
		965.6(3)	2459.22(12)	7^+	3.10(74)			5.46(47)		
		1207.0(2)	2217.82(12)	8^+	12.7(23)			22.51(86)		
		1368.0(2)	2056.80(12)	6^+	19.7(34)			34.77(11)		
		1957.6(2)	1467.23(12)	6^+	7.8(9)			13.79(83)		
3453.72(23)		994.5(3)	2459.22(12)	7^+	11.4(9)			100	0.114(9)	9.67(14)
3456.61(25)		1238.8(7)	2217.81(12)	8^+	1.256(46)			100	0.0126(5)	10.62(14)
3470.30(25)		278.9(1)	3191.40(15)	(8^-)	8.5(10)			100	0.085(10)	9.79(15)
3485.78(17)		245.3(2)	3240.46(16)		0.49(8)			11.6(11)	0.042(4)	10.08(14)
		457.4(3)	3028.42(13)	$(6, 7)^+$	1.95(44)			45.4(30)		
		920.5(4)	2565.28(12)	(7^-)	1.82(17)			43.0(29)		
3509.34(25)		222.3(6)	3287.04(15)		0.75(10)			100	0.0075(10)	10.82(15)
3515.13(13)	$(6^+, 7^-)$	551.6(2)	2963.53(13)	$(6^+, 7^-)$	16.3(11)			5.01(14)	3.14(7)	8.19(13)
		668.02(15)	2847.12(12)	(7^-)	41.4(20)			12.69(27)		
		746.0(4)	2769.18(13)	$(5,6,7^+)$	3.10(41)			0.95(5)		
		949.9(1)	2565.28(12)	(7^-)	30.0(16)			9.20(20)		
		958.9(2)	2556.23(12)	(6^-)	18.7(13)			5.73(16)		
		988.9(1)	2526.21(12)	(6^+)	78.4(53)			24.05(52)		
		1019.0(4)	2496.11(13)	5^-	7.5(8)			2.30(11)		
		1055.70(14)	2459.22(12)	7^+	20.3(11)			6.22(15)		

TABLE II. (*Continued.*)

E_{initial} (keV)	j_i^π	E_γ (keV)	E_{final} (keV)	j_f^π	I_γ	ML	δ	BR	I_β	logft
		1113.8(4)	2401.37(13)	(6^+)	3.82(50)			1.17(6)		
		1297.3(9)	2217.82(12)	8^+	10.3(8)			3.16(10)		
		2047.9(1)	1467.23(12)	6^+	96.2(32)			29.52(50)		
3519.51(13)	6^+	218.1(7)	3301.42(15)		4.67(48)			1.11(7)	4.20(8)	8.06(13)
		646.3(4)	2873.18(13)	(7^-)	16.4(10)			3.90(14)		
		672.4(4)	2847.12(12)	(7^-)	15.1(10)			3.60(14)		
		724.2(7)	2795.30(14)	8^+	2.04(25)			0.49(4)		
		842.4(1)	2677.32(13)	(5,6)	36.5(28)			8.70(41)		
		954.2(2)	2565.28(12)	(7^-)	4.39(66)			1.05(9)		
		963.3(1)	2556.23(12)	(6^-)	36.6(17)			8.72(22)		
		993.3(2)	2526.21(12)	(6^+)	25.9(23)			6.16(33)		
		1023.4(2)	2496.11(13)	5^-	18.4(15)			4.39(21)		
		1060.3(8)	2459.22(12)	7^+	5.03(50)			1.20(7)		
		1301.7(2)	2217.82(12)	8^+	6.99(62)			1.67(9)		
		2052.30(5)	1467.23(12)	6^+	248(7)	$M1, E2$	-12^{+8}_{-38}	59.01(63)		
3526.71(22)		731.4(5)	2795.30(14)	8^+	6.0(9)			37.4(27)	0.161(14)	9.48(14)
		1308.9(3)	2217.82(12)	8^+	10.0(10)			62.6(27)		
3552.84(19)		856.1(1)	2696.76(13)	(6^-)	31.8(7)			100	0.293(9)	9.20(13)
3559.12(24)		530.7(4)	3028.42(13)	$(6^+,7)$	1.09(12)			100	0.0109(11)	10.64(14)
3564.02(23)		1104.8(2)	2459.22(12)	7^+	6.26(64)			100	0.063(6)	9.87(14)
3569.05(13)	$6^+, 7$	467.4(9)	3101.70(17)		1.72(28)			0.52(6)	3.29(7)	8.14(13)
		721.9(3)	2847.12(12)	(7^-)	14.3(9)			4.35(18)		
		1003.8(1)	2565.28(12)	(7^-)	27.0(13)			8.11(22)		
		1109.8(3)	2459.22(12)	7^+	10.3(6)			3.12(12)		
		1167.7(3)	2401.37(13)	(6^+)	8.0(7)			2.44(14)		
		1351.20(14)	2217.82(12)	8^+	10.1(8)			3.06(17)		
		1512.30(13)	2056.80(12)	6^+	29.1(14)			8.84(24)		
		2101.80(4)	1467.23(12)	6^+	229(6)			69.56(44)		
3575.22(23)		1116.0(4)	2459.22(12)	7^+	5.95(59)			100	0.060(6)	9.88(14)
3597.33(23)		2130.1(2)	1467.23(12)	6^+	11.6(8)			100	0.116(8)	9.58(14)
3623.11(14)		431.7(3)	3191.40(15)	(8^-)	7.1(7)			9.37(31)	0.759(30)	8.75(14)
		594.7(2)	3028.42(13)	$(6^+,7)$	12.7(15)			16.76(62)		
		853.9(2)	2769.18(13)	$(5,6,7^+)$	9.7(10)			12.72(41)		
		1018.6(3)	2604.52(16)	$4^+, 5, 6^+$	4.77(56)			6.29(26)		
		1066.9(2)	2556.23(12)	(6^-)	14.1(9)			18.55(56)		
		1405.3(5)	2217.82(12)	8^+	15.7(17)			20.63(64)		
		1566.3(2)	2056.80(12)	6^+	11.9(12)			15.68(49)		
3628.83(16)	5,6,7	1072.6(3)	2556.23(12)	(6^-)	14.4(15)			21.4(16)	0.589(27)	8.85(14)
		2161.6(1)	1467.23(12)	6^+	52.8(21)			78.6(15)		
3634.32(19)		602.4(2)	3031.91(14)	(8^-)	1.26(14)			100	−0.0022(32)	
3639.63(15)	$5^-, 6^+, 7^+$	537.9(3)	3101.70(17)		4.07(53)			3.02(21)	1.346(39)	8.49(13)
		611.2(1)	3028.42(13)	$(6, 7)^+$	36.9(26)			27.40(81)		
		1074.4(1)	2565.28(12)	(7^-)	24.6(10)			18.28(51)		
		1083.4(2)	2556.23(12)	(6^-)	11.7(10)			8.71(37)		
		2172.4(1)	1467.23(12)	6^+	57.3(21)			42.59(85)		
3642.51(31)		570.2(2)	3072.31(23)		7.35(50)			100	0.074(5)	9.75(14)
3666.12(23)		1448.30(25)	2217.82(12)	8^+	4.85(60)			100	0.049(6)	9.92(14)
3671.52(23)		1212.3(3)	2459.22(12)	7^+	7.78(72)			100	0.078(7)	9.71(14)
3675.00(14)		522.60(27)	3152.37(15)	$7,8^+, 9^-$	12.8(9)			10.38(30)	1.233(39)	8.51(13)
		905.80(26)	2769.18(13)	$(5,6,7^+)$	3.86(44)			3.13(17)		
		1109.7(1)	2565.28(12)	(7^-)	41.9(27)			33.98(68)		
		1118.8(2)	2556.23(12)	(6^-)	4.6(7)			3.74(27)		
		1457.20(26)	2217.82(12)	8^+	21.4(17)			17.36(55)		
		2207.8(1)	1467.23(12)	6^+	38.7(17)			31.41(68)		
3682.33(18)		1464.5(2)	2217.82(12)	8^+	9.4(20)			56.3(38)	0.167(22)	9.37(15)
		2215.10(24)	1467.23(12)	6^+	7.3(10)			43.7(38)		

TABLE II. (*Continued.*)

E_{initial} (keV)	j_i^π	E_γ (keV)	E_{final} (keV)	j_f^π	I_γ	ML	δ	BR	I_β	logft
3691.68(13)	6^+,7	539.3(5)	3152.37(15)	7,8^+, 9^-	7.4(6)			1.69(5)	4.38(10)	7.95(13)
		994.90(14)	2696.76(13)	(6^-)	48.4(45)			11.06(36)		
		1126.40(5)	2565.28(12)	(7^-)	97.1(47)			22.17(35)		
		1135.4(1)	2556.23(12)	(6^-)	20.6(14)			4.70(12)		
		1165.5(1)	2526.21(12)	(6^+)	72.5(53)			16.56(39)		
		1232.5(3)	2459.22(12)	7^+	12.0(8)			2.75(7)		
		1473.9(1)	2217.82(12)	8^+	45.7(23)			10.43(19)		
		1634.9(1)	2056.80(12)	6^+	69.1(35)			15.78(27)		
		2224.4(1)	1467.23(12)	6^+	65.1(23)			14.86(26)		
3729.23(18)		1511.4(1)	2217.82(12)	8^+	8.7(15)			51.3(33)	0.170(18)	9.34(15)
		2262.0(3)	1467.23(12)	6^+	8.2(10)			48.7(33)		
3742.81(14)		714.4(2)	3028.42(13)	$(6, 7)^+$	4.64(17)			28.8(14)	0.41(6)	8.94(15)
		895.7(2)	2847.12(12)	(7^-)	16.3(52)			32.1(15)		
		973.6(5)	2769.18(13)	(5,6,7^+)	4.2(14)			8.4(5)		
		1283.6(2)	2459.22(12)	7^+	2.31(81)			4.5(4)		
		1525.0(2)	2217.82(12)	8^+	6.2(20)			12.2(8)		
		2275.6(3)	1467.23(12)	6^+	7.1(16)			14.0(15)		
3768.22(23)		1550.4(3)	2217.82(12)	8^+	4.08(55)			100	0.041(6)	9.93(15)
3773.43(23)		2306.2(3)	1467.23(12)	6^+	3.79(68)			100	0.038(7)	9.96(15)
3782.32(23)		1564.5(2)	2217.82(12)	8^+	8.1(8)			100	0.080(8)	9.63(14)
3787.01(15)		1221.6(2)	2565.28(12)	(7^-)	14.1(16)			47.4(22)	0.297(20)	9.06(14)
		2319.7(2)	1467.23(12)	6^+	15.6(11)			52.6(22)		
3816.72(23)		1598.9(3)	2217.82(12)	8^+	5.23(60)			100	0.052(6)	9.80(14)
3818.71(31)		746.4(4)	3072.31(23)		5.84(42)			100	0.058(4)	9.75(14)
3849.52(18)		1390.3(4)	2459.22(12)	7^+	9.9(12)			41.3(22)	0.240(16)	9.12(14)
		1631.7(2)	2217.82(12)	8^+	14.1(11)			58.7(22)		
3963.21(31)		890.9(5)	3072.31(23)		2.86(27)			100	0.0286(27)	9.97(14)
3974.01(31)		901.7(2)	3072.31(23)		4.71(37)			100	0.0471(37)	9.74(14)
3976.53(23)		2509.3(4)	1467.23(12)	6^+	8.07(71)			100	0.081(7)	9.52(14)
3986.81(31)		914.5(3)	3072.31(23)		7.75(52)			100	0.0775(52)	9.53(14)
4098.01(31)		1025.7(8)	3072.31(23)		2.33(24)			100	0.0233(24)	9.98(14)
4214.52(13)		427.6(4)	3787.01(15)		4.16(68)			1.87(10)	2.22(8)	7.93(14)
		580.2(2)	3634.32(19)		1.48(29)			0.66(4)		
		585.7(3)	3628.83(16)	5,6,7	8.3(11)			3.73(15)		
		661.7(2)	3552.84(19)		2.48(41)			1.12(6)		
		699.4(4)	3515.13(13)	(6^+, 7^-)	11.6(16)			5.21(22)		
		909.1(2)	3305.42(15)		5.31(89)			2.39(13)		
		913.1(3)	3301.42(15)		18.9(36)			8.51(49)		
		957.6(1)	3256.93(15)		20.4(23)			9.16(31)		
		980.0(1)	3234.51(13)	(8^+)	32.4(45)			14.56(57)		
		1023.1(2)	3191.40(15)	(8^-)	12.1(14)			5.46(20)		
		1032.3(1)	3182.22(23)		12.5(15)			5.61(21)		
		1144.5(1)	3070.01(13)	5^+, 6, 7^+	45.6(10)			20.53(73)		
		1182.6(1)	3031.91(14)	(8^-)	20.2(23)			9.07(30)		
		1186.1(2)	3028.42(13)	$(6, 7)^+$	4.13(72)			1.86(10)		
		1259.0(2)	2955.52(13)	(7^+)	16.9(30)			7.59(41)		
		1367.4(2)	2847.12(12)	(7^-)	5.92(85)			2.67(12)		
4241.22(13)		954.2(2)	3287.04(15)		14.2(50)			16.42(74)	1.57(7)	8.07(14)
		1006.7(9)	3234.51(13)	(8^+)	12.9(18)			7.58(39)		
		1171.2(3)	3070.01(13)	5^+, 6, 7^+	21.7(37)			12.73(71)		
		1238.9(7)	3002.32(14)	$(6)^+$	23.1(31)			13.57(63)		
		1277.7(2)	2963.53(13)	(6^+, 7^-)	12.7(16)			7.47(34)		
		1285.7(2)	2955.52(13)	(7^+)	18.8(34)			11.01(67)		
		1368.0(2)	2873.18(13)	(7^-)	8.1(11)			4.75(24)		
		1394.1(1)	2847.12(12)	(7^-)	24.0(26)			14.09(57)		
		1782.0(2)	2459.22(12)	7^+	21.1(17)			12.38(48)		

TABLE II. (*Continued.*)

E_{initial} (keV)	J_i^π	E_γ (keV)	E_{final} (keV)	J_f^π	I_γ	ML	δ	BR	I_β	logft
4250.29(13)		463.0(2)	3787.01(15)		9.3(13)			2.22(12)	4.21(18)	7.63(14)
		944.9(4)	3305.42(15)		14.5(26)			3.45(25)		
		1015.8(2)	3234.51(13)	(8^+)	27.7(36)			6.58(30)		
		1020.9(2)	3229.38(19)		4.50(60)			1.07(5)		
		1180.3(4)	3070.01(13)	$5^+, 6, 7^+$	18.4(31)			4.36(29)		
		1248.0(2)	3002.32(14)	$(6)^+$	67.5(77)			16.02(54)		
		1286.80(15)	2963.53(13)	$(6^+, 7^-)$	22.8(26)			5.41(20)		
		1377.1(6)	2873.18(13)	(7^-)	2.8(12)			0.68(12)		
		1403.2(1)	2847.12(12)	(7^-)	84.0(79)			19.93(45)		
		1685.10(4)	2565.28(12)	(7^-)	145(13)			34.42(65)		
		1791.1(1)	2459.22(12)	7^+	24.7(19)			5.86(16)		
4341.92(31)		1269.6(2)	3072.31(23)		3.67(31)			100	0.0367(31)	9.63(14)
4460.81(31)		1388.5(8)	3072.31(23)		4.78(37)			100	0.0478(37)	9.45(14)
4465.21(31)		1392.9(2)	3072.31(23)		2.90(27)			100	0.0290(27)	9.67(14)
4471.12(23)		2253.3(7)	2217.82(12)	8^+	2.74(41)			100	0.0274(41)	9.68(14)
4509.26(24)		1812.5(1)	2696.76(13)	(6^-)	2.90(47)			100	0.0290(47)	9.64(14)
4511.91(19)		1716.6(5)	2795.30(14)	8^+	8.9(13)			42.5(27)	0.210(17)	8.77(14)
		2294.1(2)	2217.82(12)	8^+	12.1(11)			57.5(27)		
4597.29(16)		1356.8(3)	3240.46(16)		4.7(10)			11.4(12)	0.412(47)	8.43(14)
		1362.8(4)	3234.51(13)	(8^+)	22.7(42)			55.1(21)		
		2032.0(3)	2565.28(12)	(7^-)	8.1(15)			19.8(16)		
		2138.1(2)	2459.22(12)	7^+	5.65(68)			13.7(12)		
4807.92(23)		2590.1(6)	2217.82(12)	8^+	3.32(44)			100	0.0332(44)	9.40(15)
4813.62(23)		2595.8(5)	2217.82(12)	8^+	3.48(50)			100	0.0348(50)	9.37(15)

uncertainties determined from the δ values corresponding to the $\chi^2_{\text{min}} + 1$ values. These uncertainties are generally asymmetric in nature. The mixing ratios of the transitions from the levels populated by short and long decays of ^{122}Cs are displayed in Tables I and II, respectively.

IV. RESULTS AND DISCUSSION

In the discussion below, we focus on the suggested band structures. Since the ground-state band and "K^π"$= 2^+$ band have already been well established, we focus on other band structures in ^{122}Xe.

A. Excited 0^+ states and their rotational bands

Previous to our studies, there was only one firmly assigned excited 0^+ state at 1149.3 keV [17]. In addition, a spin 1 or 2 state was known at 1716.5 keV [17] that was suggested as a 0^+ state based on energy systematics [19], and was definitively established as such [28,30] based on the γ-γ angular correlation analysis. In the present study, the angular correlation analysis has been extended to include all γ rays with sufficient intensity that feed the 2_1^+ level. Figure 7 displays the spectrum observed from the short-cycle data with a coincidence condition placed on the 331.2 keV $2_1^+ \rightarrow 0_1^+$ γ ray. The peaks for which sufficient intensity was observed for a γ-γ angular correlation analysis are identified, as well as other γ-ray transitions of significance. In total, eleven excited 0^+ states have been firmly identified using the γ-γ correlations, examples of which are shown in Figs. 11 and 12. All correlations are displayed in the Supplemental Material [37].

The 2^+ members of the 0_2^+ and 0_3^+ bands were also established in Refs. [28,30] with the observation of the in-band $2^+ \rightarrow 0^+$ transitions. A state has been established at 1854 keV that decays to the 2_1^+, 2_2^+, and 4_1^+ levels, and is fed by transitions from levels favored to have $I^\pi = 6^+$ assignments. We thus assign $I^\pi = 4^+$ for this level. The 4^+ spin assignment is also strongly favored by the γ-γ angular correlations as shown in Fig. 8. The spin 5 and 6 solutions can be immediately rejected since the 1854.5 keV level decays to 2^+ states. This level is fed by a 546.9 keV γ ray from a level at 2401.4 keV with a tentative $I^\pi = 6^+$ assignment that is a candidate for the 6^+ rotational band member. The 2401.4 keV state also possess a decay to the 1920.6 keV level that is also favored to be a 4^+ state. The 1920.6 keV level has a branch to the 2_2^+ level of magnitude similar to that of the 1854.5 keV state. Thus, from the branching ratios alone we cannot firmly assign the 4^+ member of the 0_2^+ band, and it appears that both the 1854.5 and 1920.6 keV levels are mixed. However, as will be discussed below, considering the energy systematics and especially the energy staggering, we assign the 1920.6 keV level as the head of a $K^\pi = 4^+$ band.

A new 0^+ state has been established at 1788.1 keV that decays with a 1456.8 keV transition, which feeds the 2_1^+ state, and a 944.9 keV γ ray, which feeds the 2_2^+ state. The portion of the γ-ray spectrum obtained with a coincidence condition on the 944.9 keV $0_4^+ \rightarrow 2_2^+$ γ ray is shown in Fig. 9. A weak peak is observed at 476.3 keV from a newly established 2264.4 keV state. The 2264.4 keV state is firmly assigned as a

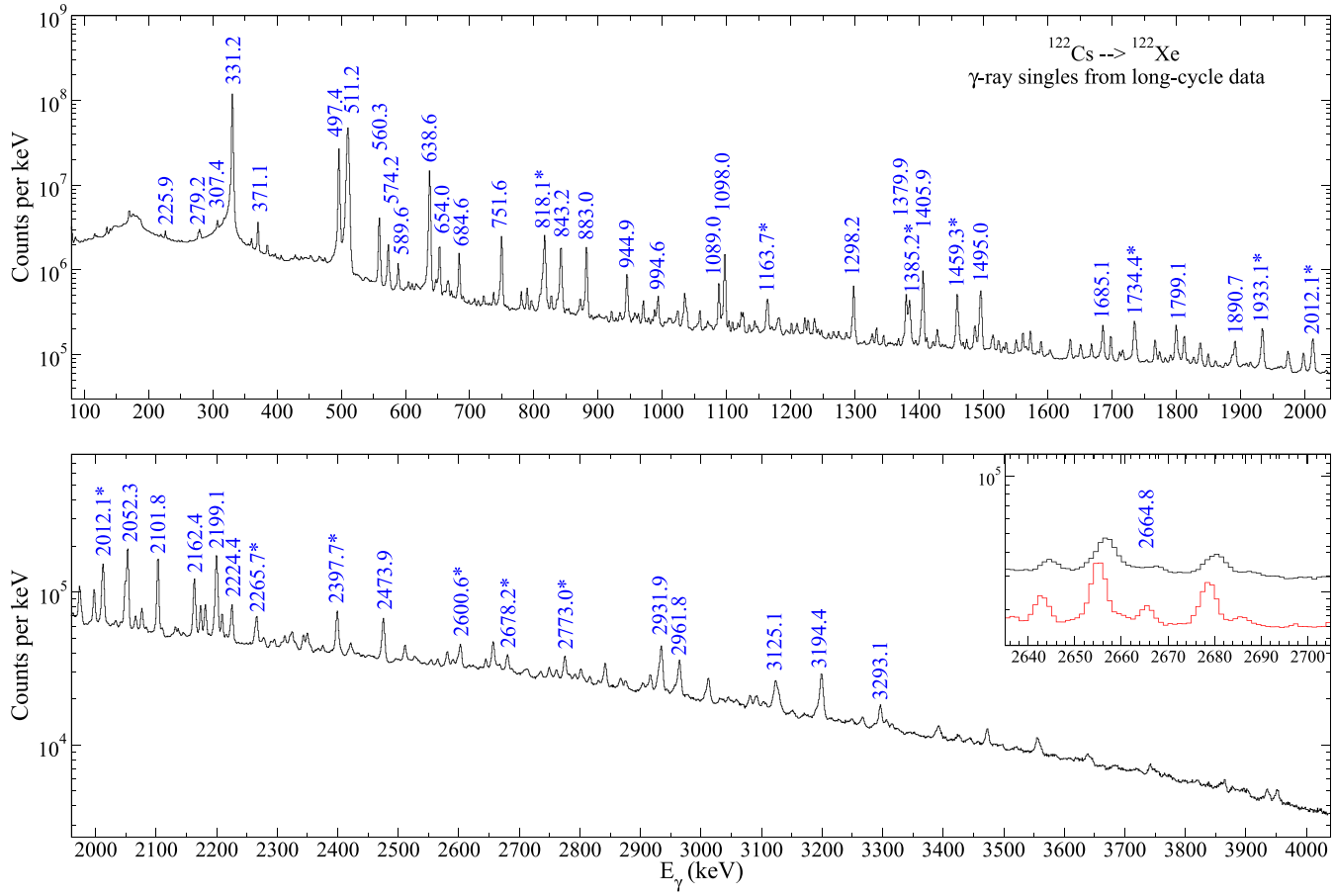

FIG. 5. The γ-ray singles spectrum observed following the decay of the $8^{(-)}$ ^{122}Cs^m state. The spectrum was generated by placing a condition on the collected data accepting events with clock times $T > 150$ s following the implantation of the ^{122}Cs beam. The prominent peaks are labeled with the energies in keV and the γ rays used for an angular correlation analysis are indicated by an asterisk. The inset displays the region of the spectrum in the vicinity of 2664.8 keV to display the effect of placing the time condition on the data; the spectrum in black has no time conditions, whereas the one in red has the $T > 150$ s condition. The complexity of the spectrum is evident with the majority of peaks having an unresolved doublet nature with transitions resulting from the low-spin decay.

2^+ state from the angular correlation of the 1933.1-331.2 keV γ-γ cascade, shown in Fig. 10, and we thus assign the 2264.4 keV state as the 2^+ rotational band member of the 0^+_4 band.

The partial level scheme displaying the assigned 0^+ rotational bands is shown in Fig. 13. Unfortunately, we cannot firmly assign rotational band members to higher-lying 0^+states, despite there being many candidates, due to the lack of observation of in-band transitions. One notices a trend, however, of increasing $2^+ \rightarrow 0^+$ spacing with increasing excitation energy. The next higher-lying excited 0^+ state, at 2304.0 keV, therefore likely has its associated 2^+ rotational band member in the vicinity of 2.8 MeV, and is unlikely to have it located below 2.6 MeV.

B. Excited $K^\pi = 2^+$ bands

The first $K = 2$ band, based on the 2^+_2 state at 843.2 keV, is well established up to the $I^\pi = 15^+$ state [17]. The 2^+_2 level has the strongest decay branch, at 511.2 keV, to the 2^+_1 state with an evaluated value of 100 ± 16 relative to the ground-state branch at 843.2 keV of 45 ± 8. In the present work, the 511.2 keV branch is definitely observed but the large abundance of the 511 keV annihilation radiation makes the determination of its branching ratio highly suspect. Thus, we report only upper limits on its transition intensity in Tables I and II.

As outline above, all unassigned 2^+ states below 2.6 MeV must either be associated with $K = 1$ bands or act as bandheads of $K = 2$ bands, under the assumption that we have detected all excited 0^+ states below 2.3 MeV. Firmly assigned 2^+ states above the 2^+_2 $K = 2$ bandhead, which have not been assigned as belonging to 0^+ bands include the levels at 1882.0 and 2047.0 keV. There are also levels at 2223.8, 2249.1, and 2285.0 keV that do not have firm spin assignments and could be considered as possible 2^+ states.

The 2^+_4 state at 1882.0 keV is assigned as an excited $K = 2$ bandhead. Its decay is highly fragmented, and we have mixing ratios δ for the transition to the 2^+_1 level, $\delta = -1.2^{+0.5}_{-0.4}$, indicating a slight preference for $E2$ multipolarity, and to the 2^+_2 level with $\delta = 0.4(1)$ indicating a mostly $M1$ multipolarity. Using the spacing of the $K^\pi = 2^+_1$ band as a guide, the 3^+ member is expected at 2252 keV. A candidate state is located at 2249.1 keV that is extremely weakly populated

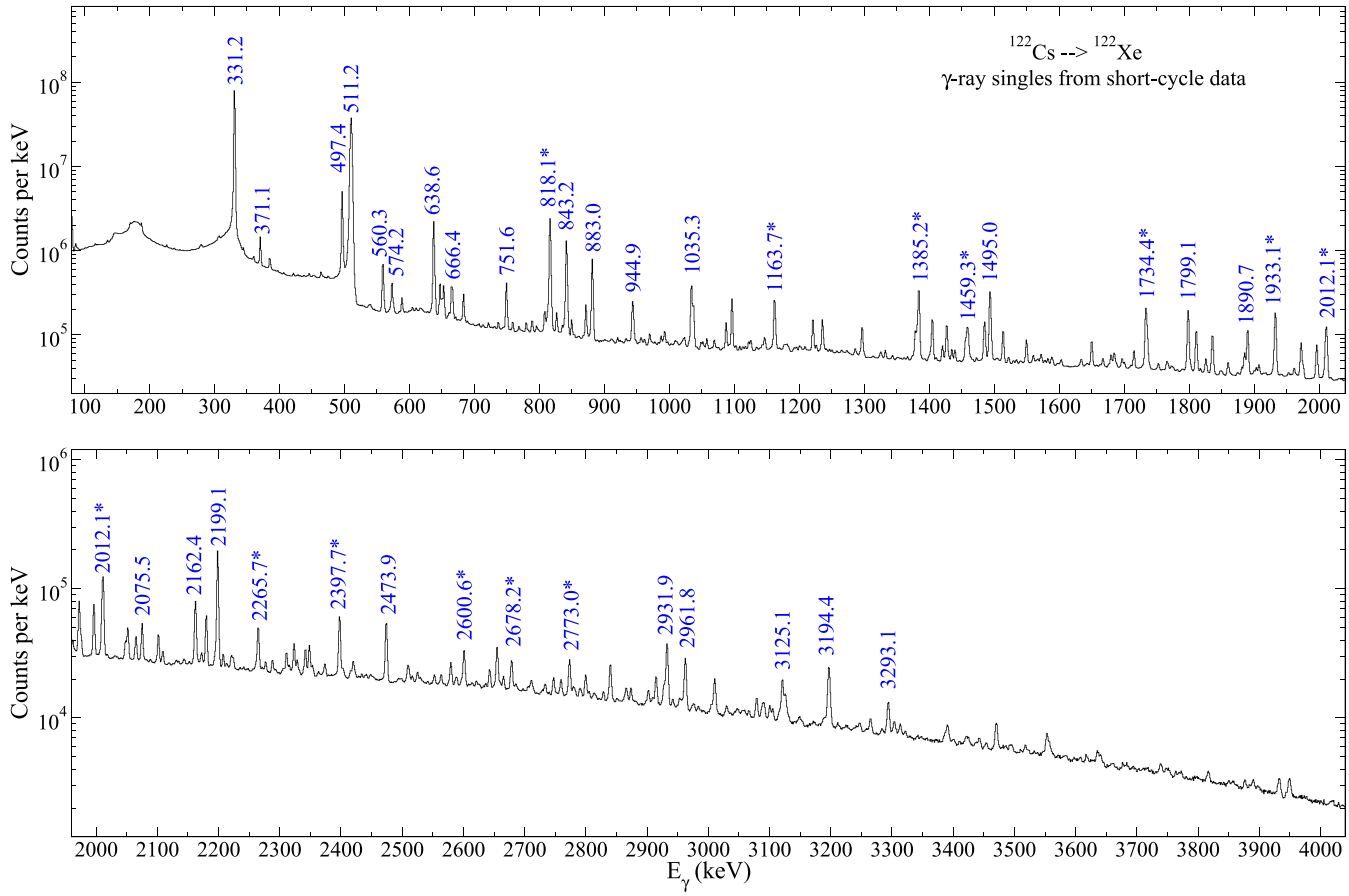

FIG. 6. The γ-ray singles spectrum observed following the decay of the 1^+ ^{122}Cs ground state, obtained from the short-tape-cycle data. Some of the prominent γ rays observed are labeled with their energy in keV, and the γ rays used for an angular correlation analysis are indicated by asterisk.

in the ^{136}Cs 1^+ decay, and which has an observable decay to the 3_1^+ state only. No candidates for higher-lying band members could be identified. We also note that the excitation energy of the 1882.0 keV state is reasonably close to the sum $E(0_2^+) + E(2_2^+) = 1992$ keV. The observed decays to both the 2_3^+ and 0_2^+ states may be taken as evidence of the 1882.0 keV state as an excitation built on the 0_2^+ level, especially considering that the $B(E2)$ ratio favors decay to the 0_2^+ state over that to the ground state by a factor of ≈32.

The level at 2012.1 keV is favored to have spin 1. As shown by von Garrel *et al.* [11], the quadrupole-octupole coupled 1^- excitation is expected to lie at an energy of ≈2.36 MeV in ^{124}Xe, and in ^{122}Xe this excitation is expected at 2149 keV using our newly assigned 3_1^- state (discussed below), thus higher than the candidate spin 1 state at 2012.1 keV. Alternatively, the 2012.1 keV state may have $I^\pi = 1^+$, and form the head of a $K = 1$ rotational band. Considering this possibility, however, it would be unlikely that the 2^+ state at 2047.0 keV is a member of its rotational band as it would lead to a drastically reduced moment of inertia. Therefore, the 2047.0 keV state must be considered as another $K = 2$ bandhead. No excited rotational band members can be assigned given the data at hand.

C. The $K^\pi = 4^+$ band

A "$K = 4$" band has been assigned in both ^{124}Xe [9] and ^{126}Xe [44], with bandheads at 1873 and 1903 keV, respectively. In the present work, a newly observed level is established at 1920.6 keV which decays to the 2_1^+, 2_2^+, and 3_1^+ states, as can be seen in Figs. 2–4, respectively. There were insufficient statistics to permit meaningful γ-γ angular correlations for decays from this level. However, it is fed from higher-lying states that are strongly favored to have spin 6^+, such as the 2526.2 keV level, that would restrict its spin to 4^+. This level is assigned as a head of a new band with $K = 4$.

Shown in Fig. 14 is a portion of the γ-ray spectrum in coincidence with the 1589.9 keV $(4_4^+) \rightarrow 2_1^+$ transition, displaying the observed γ rays that are assigned as in-band transitions for the $K = 4$ band based on the 1920.6 keV level. These newly observed levels are established by multiple decaying transitions, as shown in Fig. 15. We suggest that the levels at 2379.6, 2526.2, and 2955.5 keV are the 5^+, 6^+, and 7^+ band members of the $K = 4$ band. A higher-lying state, at 3234.5 keV, possesses a strong branch for decay to the assigned 6^+ band member at 2526.2 keV. From its decay properties, with decays to lower-lying spin 6, 7, and 8 states only, we tentatively suggest that it is the spin 8 member of the $K = 4$ band. As shown in Fig. 15, there is a remarkably

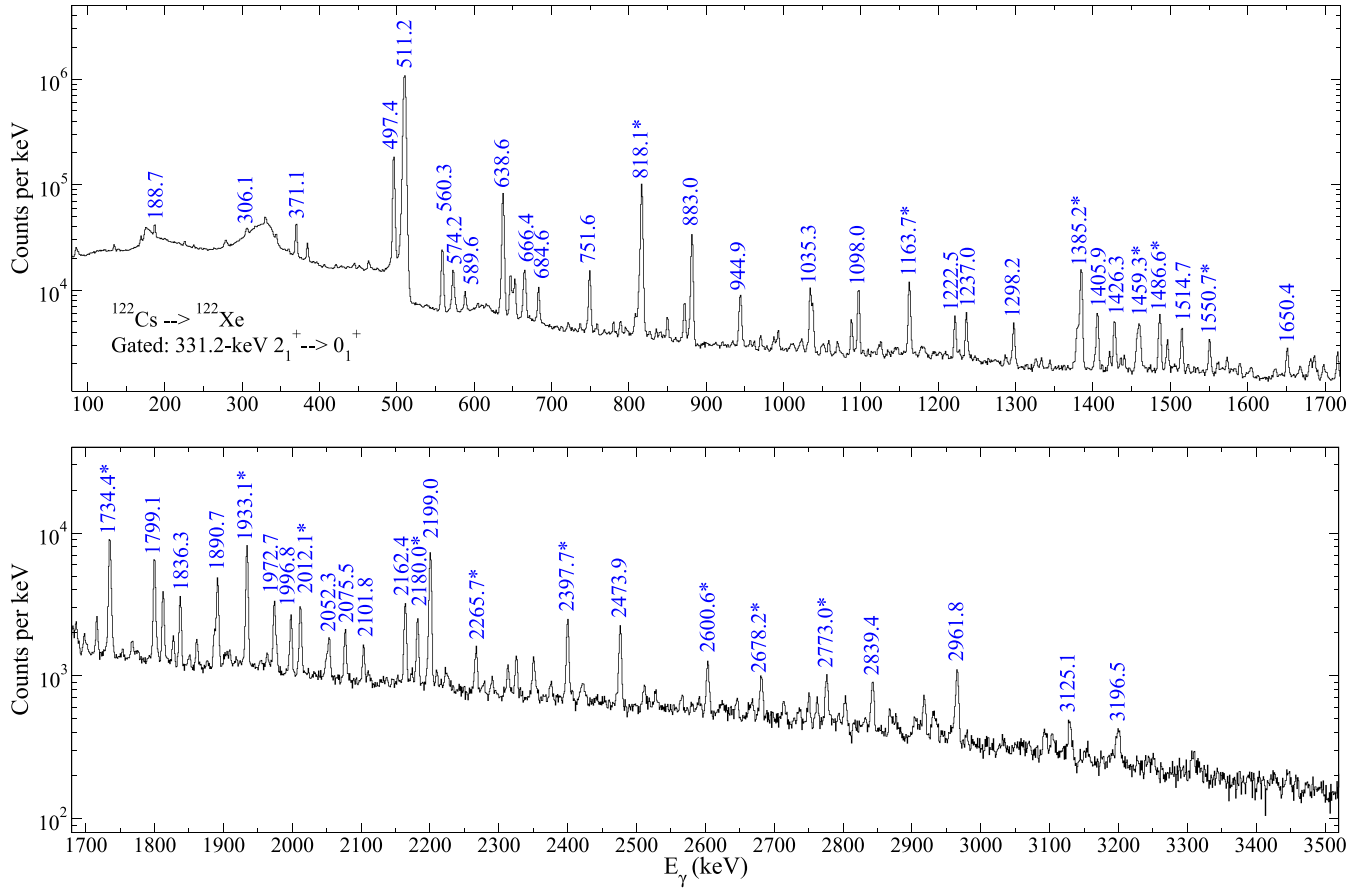

FIG. 7. Portion of the γ-ray spectrum observed from the short-cycle data with a coincidence condition placed on the 331.2 keV $2_1^+ \rightarrow 0_1^+$ γ ray. The γ rays observed with sufficient intensity are labeled with their energy in keV and the γ rays used for an angular correlation analysis are indicated by asterisk.

similarity between the assigned $K = 4$ structures in ^{122}Xe and ^{124}Xe.

Figure 16 displays the staggering, defined as

$$S(J) = \frac{E(J) - 2E(J-1) + E(J-2)}{E(2_1^+)}, \qquad (7)$$

observed in the $K = 2$ bands and the $K = 4$ bands in ^{122,124}Xe. As can be seen, the staggering is nearly identical in the $K = 2$ bands and in the newly established $K = 4$ band in ^{122}Xe with its counterpart in ^{124}Xe, although only the $S(6)$ and $S(7)$ values are known for the latter. It is this nearly identical pattern of the staggering in the $K = 4$ band that led us to favor the 1920.6 keV state as the 4^+ bandhead, although as noted above, it appears to be strongly mixed with the 1854.5 keV 4^+ member of the $K^\pi = 0_2^+$ band.

D. Assignment of negative-parity states

The most extensive investigation of the negative-parity structures in ^{122}Xe arose from the study by Timmers *et al.* [45]. In that work, the level structure of ^{122}Xe was investigated using the heavy-ion fusion evaporation reaction ^{96}Zr(^{30}Si, $4n$)^{122}Xe. Four negative-parity bands were assigned, based on a 7^- state at 2565.3 keV, the 7^- state at 2873.2 keV, the 9^- state at 3243.0 keV, and the $10^{(-)}$ state at 3599 keV. The decay of the high-spin $8^{(-)}$ isomer in ^{122}Cs provides access to the states in ^{122}Xe with a moderate amount of angular momentum, and we observe the 7^- and 9^- states cited above. We also expect that lower-spin negative-parity states will be populated through the decay of the higher-spin states. In the following, we use known systematics of the neighboring Xe isotopes combined with the decay patterns and γ-γ angular correlations in order to make the assignments.

1. The $K^\pi = 3_1^-$ band

In the latest evaluation for ^{122}Xe [17], the 3_1^- level remained unassigned. As shown in Fig. 17, candidates for the 3_1^- states are descending in energy as the neutron number decreases from $N = 74$ to $N = 70$, and based on this trend it can be expected that the 3_1^- level in ^{122}Xe should be at approximately 1.8 MeV excitation energy. The 3^- states also have the pattern in their decay of the most intense γ-ray branch to the 2_1^+ state, with a branch to the 4_1^+ state approximately an order of magnitude weaker. A new level in ^{122}Xe was observed at 1817.9 keV in both the ^{122}Cs 1^+ ground-state decay and the $8^{(-)}$ isomer decay, and its decay pattern matched well those

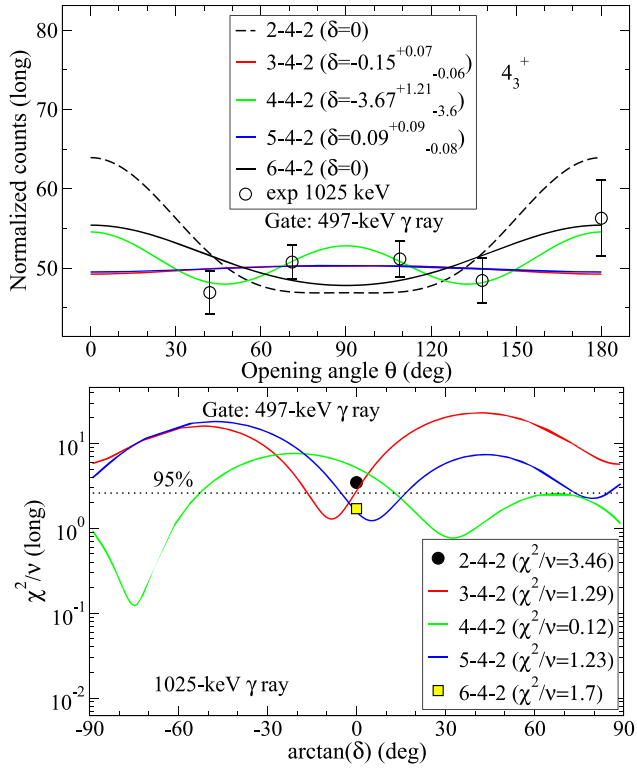

FIG. 8. Angular correlation for the 1025.4-497.4 keV γ-γ cascade. The top panel shows the intensity distribution, while the bottom panel displays the χ^2 analysis as a function of the initial state spin and mixing ratio for the 1025.4 keV γ-ray transition.

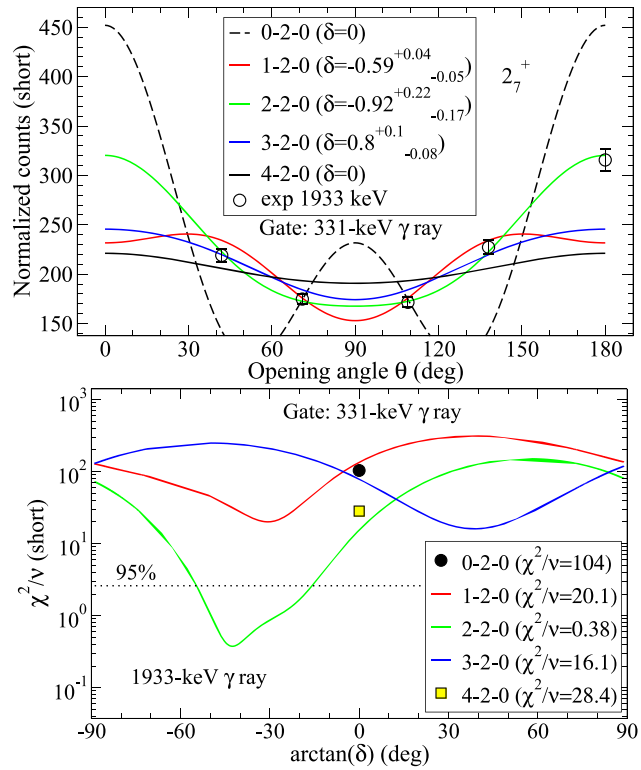

FIG. 10. Angular correlation for the 1933.1-331.2 keV γ-γ cascade. The top panel shows the intensity distribution, while the bottom panel displays the χ^2 analysis as a function of the initial state spin and mixing ratio for the 1933.1 keV γ-ray transition.

of the 3^- states in the heavier Xe isotopes. The γ-γ angular correlation for the 1486.6-331.2 keV γ-ray cascade, shown in Fig. 18, permits the 1^+, 2^+, or spin 3 solutions, with the latter solution having the χ^2 minimum located at $\delta = -0.02$. The 1^+ solution can be rejected due to the decay of the 1817.9 keV level to the 4_1^+ state. Based on the energy systematics, the decay pattern, and the γ-γ angular correlation, the 1817.9 keV level is strongly favored as the 3_1^- state in ^{122}Xe, and we make this assignment.

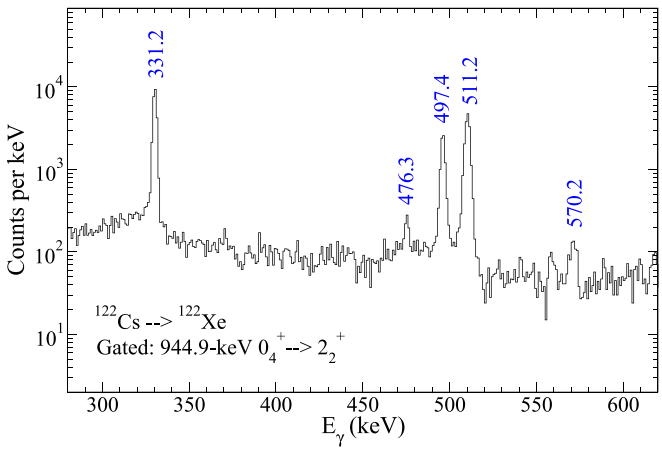

FIG. 9. Portion of the γ-ray spectrum observed from the short-cycle data with a coincidence condition placed on the 944.9 keV $0_4^+ \rightarrow 2_2^+$ γ ray. The 476.3 keV γ ray is assigned as the $2^+ \rightarrow 0_4^+$ in-band transition.

In ^{126}Xe, a band based on the 3_1^- state was assigned that included the 5_2^- level at 2414 keV, the 7_3^- level at 2881 keV, etc., as shown in Fig. 19. In ^{124}Xe, a similar structure is proposed [46], with the 5_1^- level at 2227 keV and the 7_2^- level at 2676 keV. With the decrease in energy of the 3^- state in ^{122}Xe, and the larger moment of inertia observed in the ground-state band for ^{122}Xe compared to that in ^{124,126}Xe, it would be expected that the higher-spin band members will also be lower in energy. A new level was observed at 2126.8 keV that decays to the 4^+ and 6^+ ground-state-band members, as well as the 4^+ member of the γ band. The γ-γ angular correlation for the 1298.2-497.4 keV cascade, shown in Fig. 18 permits solutions with spin 3, 4, or 5. The spin 3 solution is rejected due to the level's decay to the 6^+ state, and the spin 4 solution would only be viable with a large mixing ratio δ, thus implying that it would be a 4^+ state. However, a 4^+ state would be expected to have a branch to a lower-lying 2^+ state, which has not been observed. We thus assign the spin of the 2126.8 keV level as 5. Noting further that the spin 5 solution has a minimum of its χ^2 distribution for $\delta = 0.03$, i.e., a nearly pure dipole transition, we strongly favor the assignment of 5^-. The $5^- \rightarrow 3^-$ spacing is 309 keV in ^{122}Xe, 329 keV in ^{124}Xe, and 410 keV in ^{126}Xe, following the trend of the

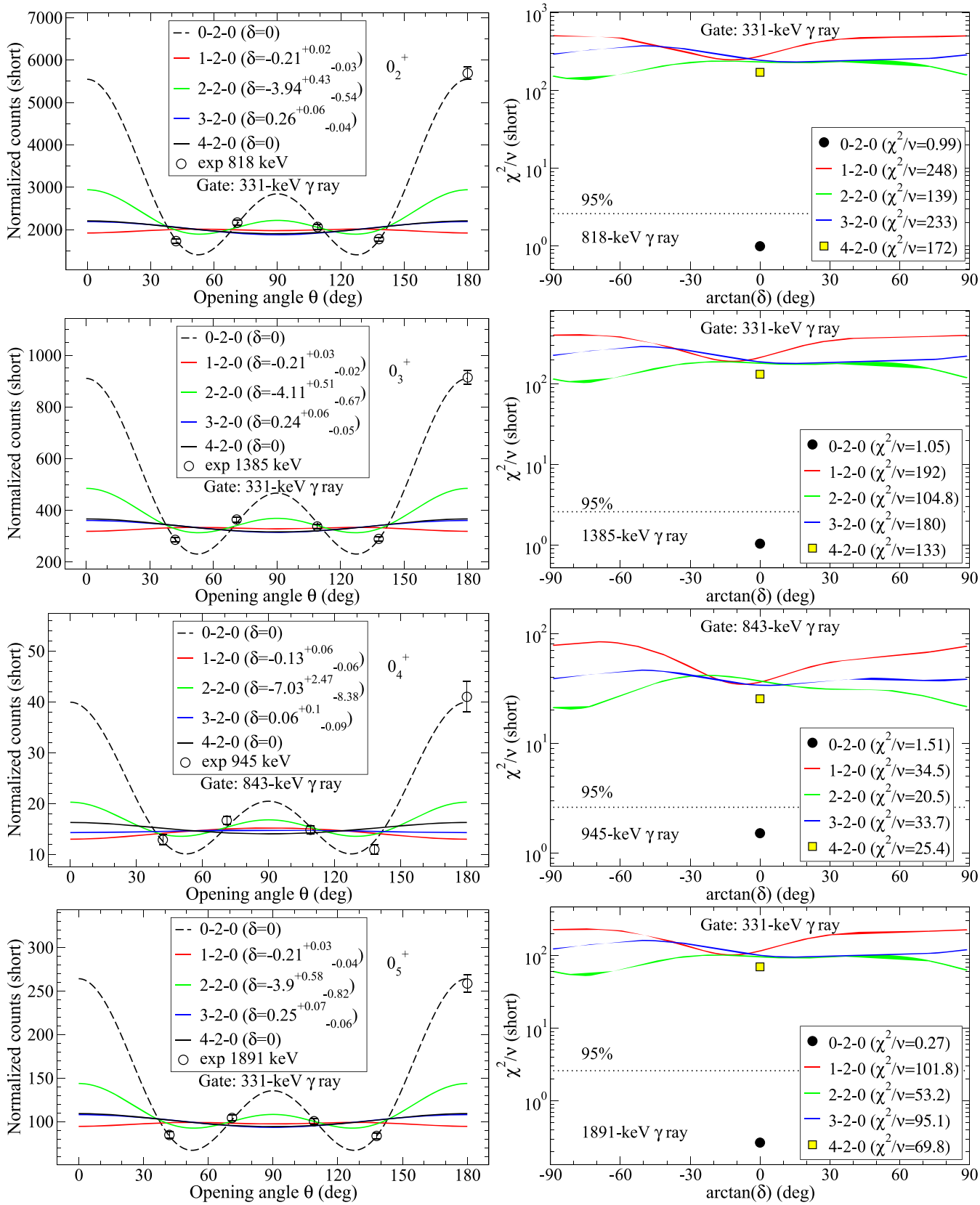

FIG. 11. Examples of γ-γ angular correlations along with their χ^2 fits for states assigned as $I^\pi = 0^+_{2-5}$.

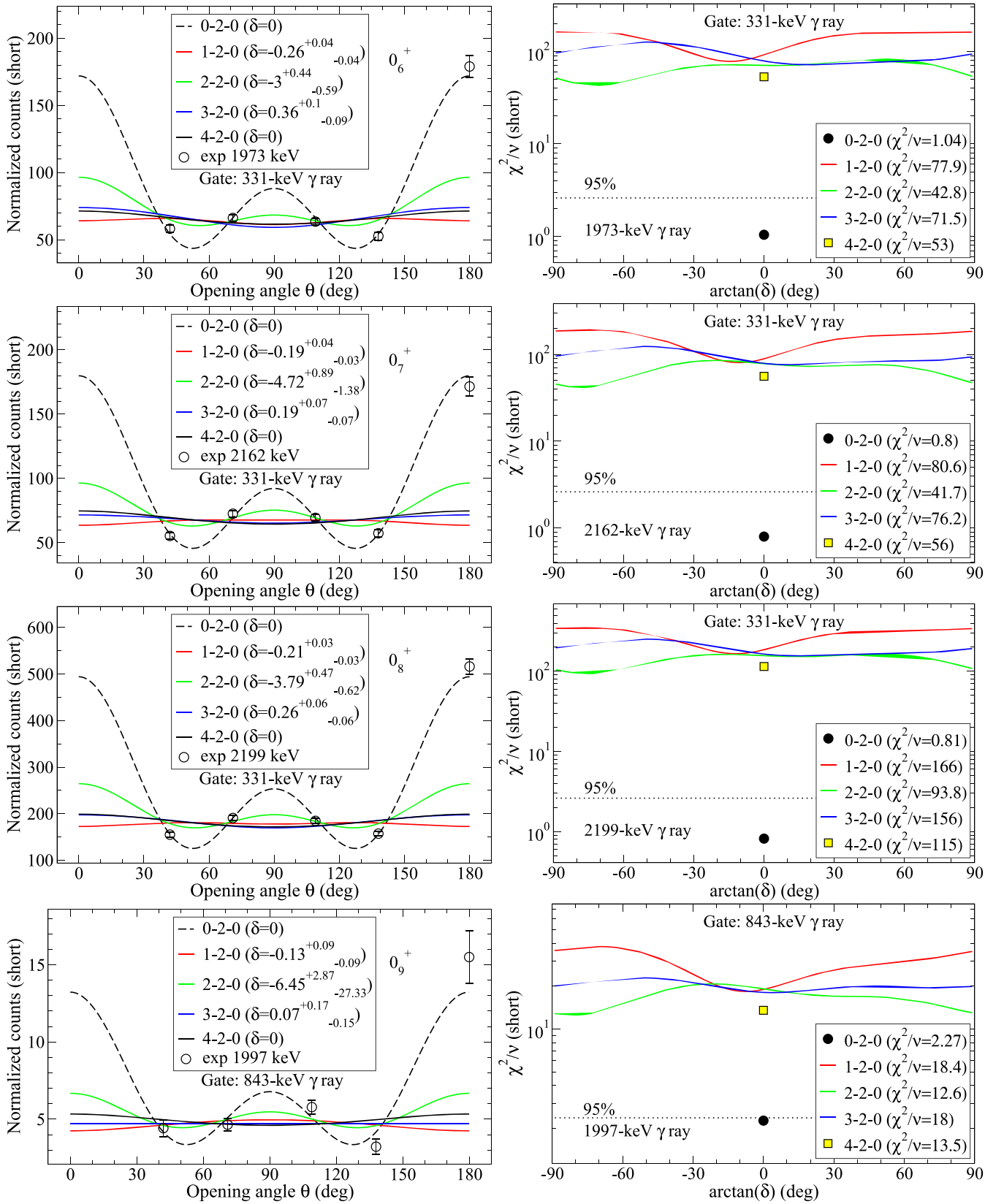

FIG. 12. Examples of γ-γ angular correlations along with their χ^2 fits for states assigned as $I^\pi = 0^+_{6-9}$.

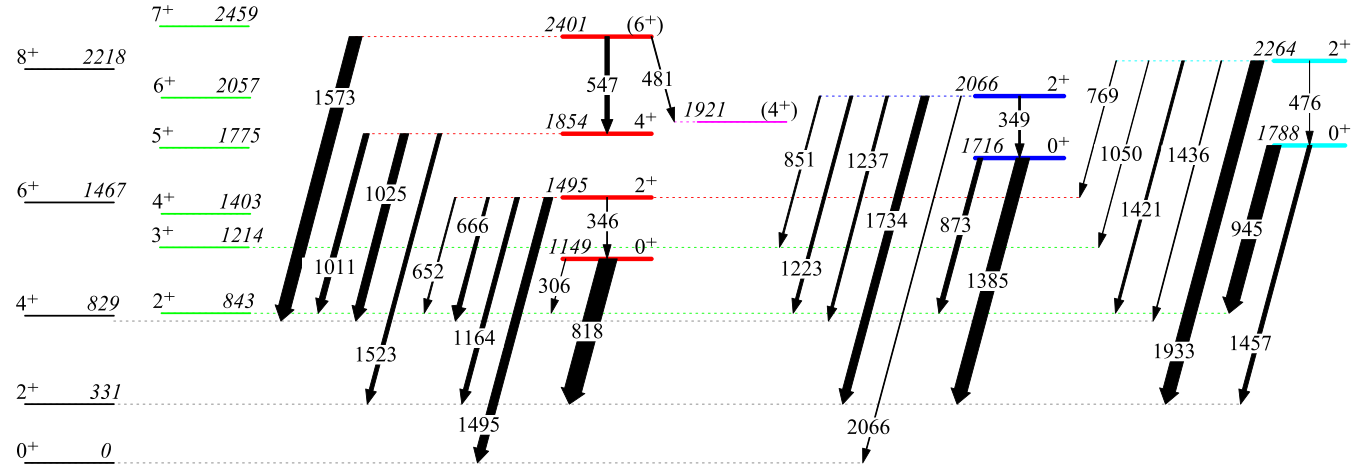

FIG. 13. Partial level scheme displaying the assigned 0^+ rotational bands in ^{122}Xe. The γ-ray transitions are represented by arrows that are labeled with their energies in keV and whose widths are proportional to the measured branching ratios.

$2^+ \rightarrow 0^+$ spacing in the ground-state bands. We thus assign this level as a member of the 3^- band.

The previously known 7^- level at 2565.3 keV has an evaluated half-life of 0.55(28) ps [18]. In the present study, we observed a new transition of 438.4 keV decaying from this level feeding the 2126.8 keV level, and thus is an $E2$ transition with $B(E2; 7^- \rightarrow 5^-) = 58(30)$ W.u. assuming the spin-parity assignment of 5^- for the 2126.8 keV state. Therefore, the band observed in Ref. [45] based on the 7^- state at 2565.3 keV is extended downwards to the 3^- state in the present work, as shown in Fig. 22.

2. The $K^\pi = 5^-$ band

In ^{126}Xe, a band was observed to be built on the 5^- state at 2302 keV, with its partner built on the 6^- state at 2562 keV [20]. These bands have not been identified in ^{124}Xe, although a candidate 5^- bandhead is observed at 2381 keV [46]. In the present work, a new level is established at 2496.1 keV based on the γ-ray coincidence data presented in Fig. 20; the 1667.5 keV γ ray feeds the 828.6 keV 4_1^+ state that decays by the 497.4 and 331.2 keV cascade to the ground state. While the angular correlations presented in Fig. 18 for the 2496.1 keV level do not permit a unique spin assignment, the decay of the level proceeds only to lower-lying 4^+ states. This is highly unlikely for a spin 3 state, of either parity, as well as for a 4^+ state (the angular correlation rules out a 4^- assignment which would need to have $\delta = 0$). The spin 5 solution has its χ^2 minimum at $\delta = -0.02(11)$, consistent with 0 as expected for a negative-parity assignment. Thus, the 2496.1 keV level is assigned as the 5_2^- state and is a natural candidate for the $K^\pi = 5^-$ bandhead. The γ-ray spectrum in coincidence with the 1667.5 keV transition from the 2496.1 keV level, shown in Fig. 20, provides clear evidence for feeding transitions at 200.7 and 377.1 keV that originate from levels at 2696.8 and 2873.2 keV, respectively. These levels are assigned as the 6^- head of the signature partner, and the 7^- band member, with the higher-spin members assigned as shown in Fig. 22. From the decay patterns, these levels appear to be highly mixed with those from the $K^\pi = 7^-$ band, discussed below, such that their assignment to a particular structure must not be considered unique.

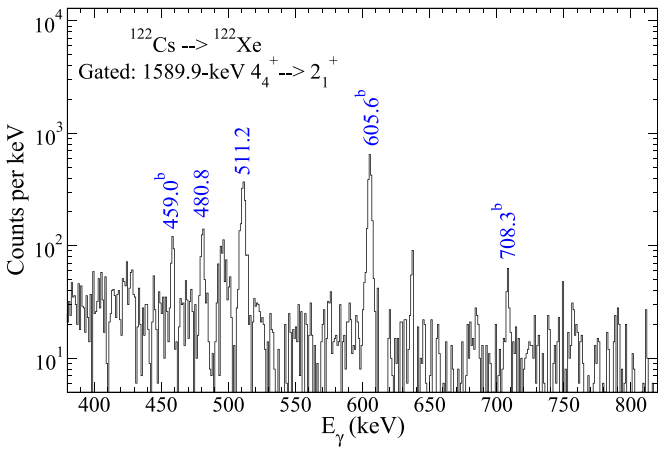

FIG. 14. Portion of the γ-ray spectrum observed in coincidence with the 1589.9 keV $4_4^+ \rightarrow 2_1^+$ transition. The γ rays observed are labeled with their energy in keV and the peaks labeled with superscript "b" are in-band transitions of the assigned $K^\pi = 4^+$ band.

3. The $K^\pi = 7^-$ band

A band built on a 7^- state, with its partner built on an 8^- state, was assigned in both ^{126}Xe and ^{124}Xe [18,20]. In ^{122}Xe, bands were assigned built on the 2873.2 keV 7^- state and the 3008.8 keV 8^- state by Timmers *et al.* [45]. In the present study, a new 7^- state is assigned at 2847.1 keV. Both the 2847.1 keV level and the 2873.2 keV level have depopulating transitions that feed many of the same lower-lying states, and are also both fed from the higher-lying states that were previously assigned as members of the 7^- band. We have a preference that the 2873.2 keV state is the member of the $K^\pi = 5^-$ band due to the presence of decays to both the 5_2^- state and to the proposed 6^- signature partner at 2696.8 keV. However, as displayed in Fig. 22, the presence of significant decay branches from the (7^-) and (8^-) states at 2847.1 and

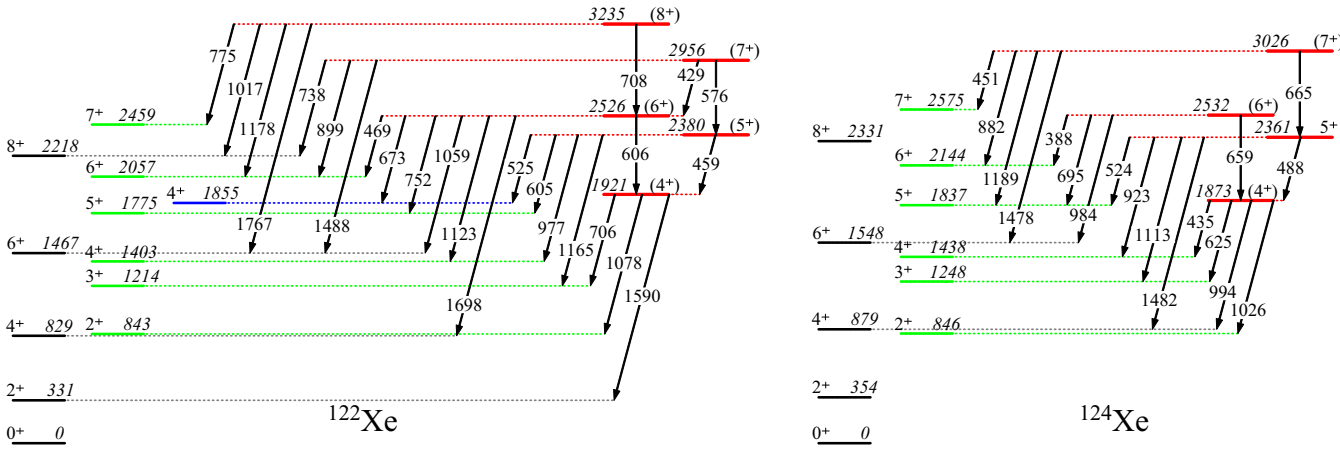

FIG. 15. Partial level schemes for ^{122}Xe (left) and ^{124}Xe (right) highlighting the assigned $K = 4$ bands. The γ-ray transitions are represented by arrows that are labeled with the energies in keV. The assignment of the band in ^{122}Xe is supported by the similarity to the known $K = 4$ band in ^{124}Xe from Ref. [9].

3008.8 keV to the 2496.1 keV 5^-, 2696.8 keV (6^-), and 2873.2 keV (7^-) states suggests substantial mixing of members of the rotational bands. It should be noted that the states assigned to the $K^\pi = 7^-$ band at 3008.8 keV and above are those of Timmers *et al.* [45]. The particular assignment of the states to either the $K^\pi = 5^-$ or 7^- band structures must await additional data such as the mixing ratios of the low-energy interband transitions and, most importantly, level lifetimes to ascertain the strength of the in-band $E2$ transitions.

E. Properties of the negative-parity bands

The level energy systematics of the negative-parity bands for ^{122,124,126}Xe are shown in Fig. 19. While the 3^-_1 state migrates slowly downwards in energy from ^{126}Xe to ^{122}Xe, the assigned $K^\pi = 5^-$ bandhead migrates upwards, as does the $K^\pi = 7^-$ bandhead. As it has been demonstrated that there is a strong correlation of the 3^- excitation energy and the $B(E3)$ value in the Xe isotopes [47], it is anticipated that the $B(E3)$ value for excitation of the 3^-_1 state will be slightly larger in ^{122}Xe than that for ^{124}Xe. In ^{124}Xe, the $B(E3; 3^-_1 \rightarrow 0^+_1)$ value reflects a collective nature with a weighted average of two measurements [10,47] of 15.0 ± 1.4 W.u. The increasing collectivity is associated with increasing interaction of $\Delta l = \Delta j = 3$ orbitals, mostly involving the $\nu h_{11/2}$ orbital.

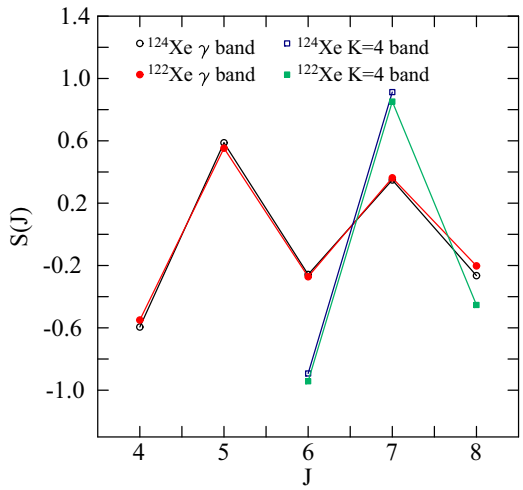

FIG. 16. Energy staggering, defined by Eq. (7), observed in the $K = 2$ bands and $K = 4$ bands in ^{122,124}Xe.

The energies of the negative-parity structures observed minus a rigid-rotor reference, calculated with a rotational parameter of 10.8 keV, are shown in Fig. 21. The 3^- and 4^- signature partners have an approximately 200 keV splitting until spin 21 when a decrease is observed. The decrease is possibly due to the influence of another configuration crossing the 3^- signature band at spin 23 resulting in the "splitting" of the sequence into two branches [45]. The 7^- and 8^- signature partners, on the other hand, are nearly degenerate until spin 16 when they begin to slowly diverge, with both signatures retaining a smooth evolution. The 5^- and 6^- partner bands are insufficiently developed to observe any trends with spin, although they appear to start with overlapping values.

Figure 23 displays the kinematic moment of inertia (MoI) for the negative-parity $K^\pi = 3^-$ and 7^- bands together with the ground-state band. The Harris parameters used were those of Ref. [45] with $J_0 = 9$ keV and $J_2 = 33$ keV chosen so that the MoI of the S band above the ground-state band back bend was approximately constant, as shown. Several features are immediately noticeable: (1) at approximately $\hbar\omega \simeq 375$ keV, a significant change in the MoI is observed for both the 3^- and 4^- signature partners, explained in Ref. [45] as a crossing of the $5/2[402] + 1/2[411] \otimes 1/2[550]$ two-quasiproton configuration with the $7/2[523] \otimes 7/2[523]$ two-quasineutron configuration; (2) at a lower frequency, there is a localized departure from the smooth behavior for the 3^- signature partner whose origin is unknown; and (3) the energy of the $K^\pi = 7^-$ bandhead, assigned at 2847.1 keV, appears to be high, resulting in a very large MoI. The complicated decay paths of the states and the inter-connectivity of the bands, as mentioned above, suggests a substantial mixing occurs that may be the underlying cause of the departure from smooth behavior of the MoIs.

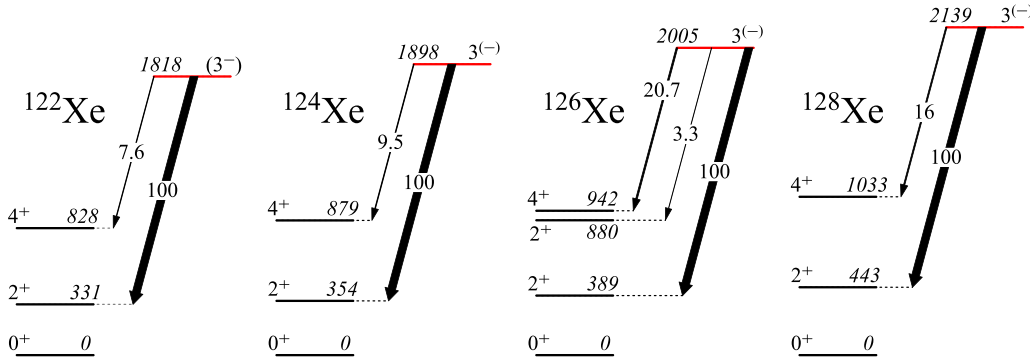

FIG. 17. Systematics of the 3_1^- states assigned in $^{122-128}$Xe. Data for ^{124}Xe are taken from Refs. [18,46], whereas those for ^{126}Xe are from Ref. [20].

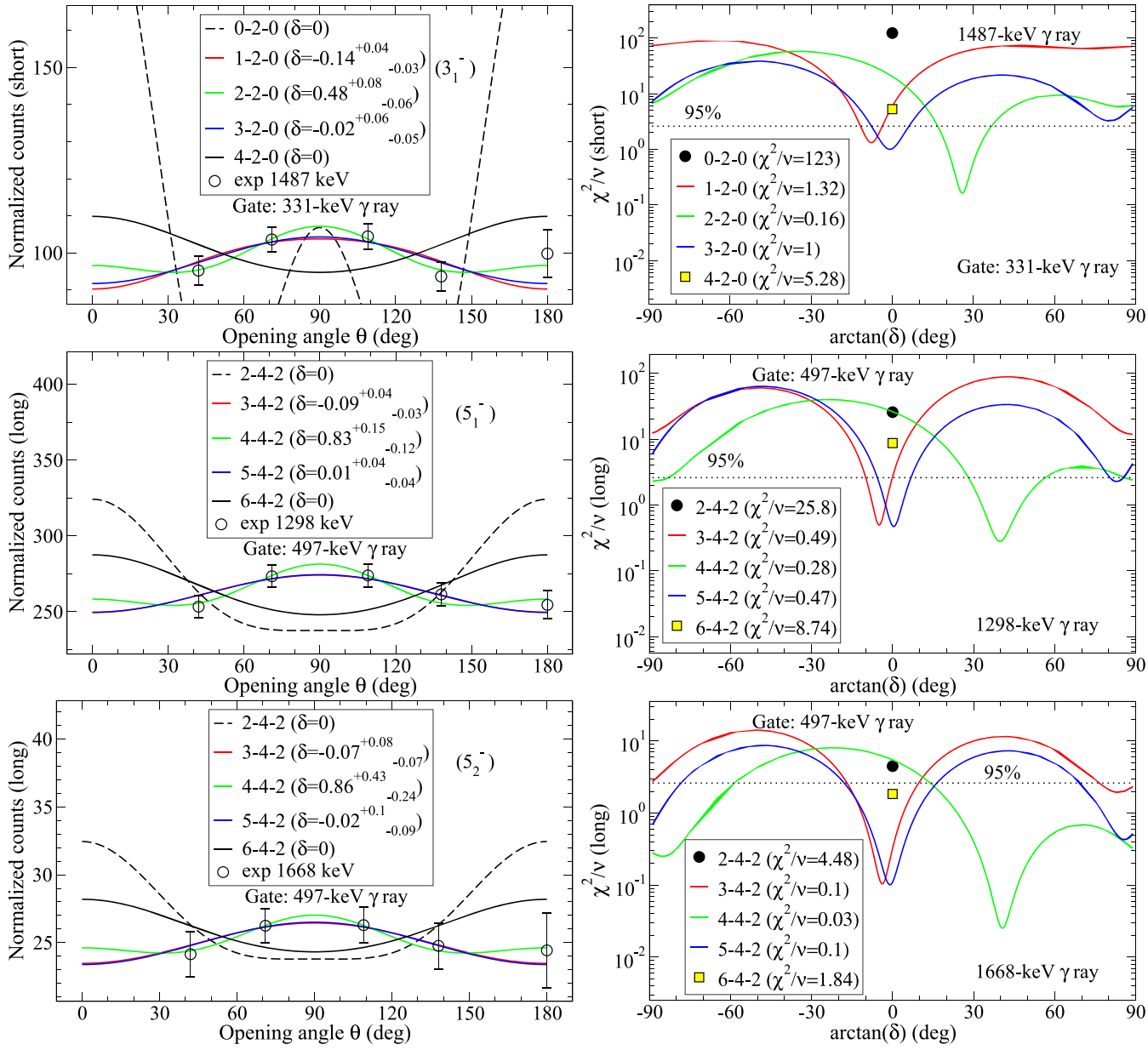

FIG. 18. The γ-γ angular correlation data for the 1486.6-331.2 keV cascade (a), the 1298.2-497.4 keV cascade (b), and the 1667.5-497.4 keV cascade (c). From consideration of the decay patterns, and the angular correlations, the 1817.9, 2126.8, and 2496.1 keV levels are assigned as the 3_1^-, 5_1^-, 5_2^- negative-parity states in ^{122}Xe. See text for details.

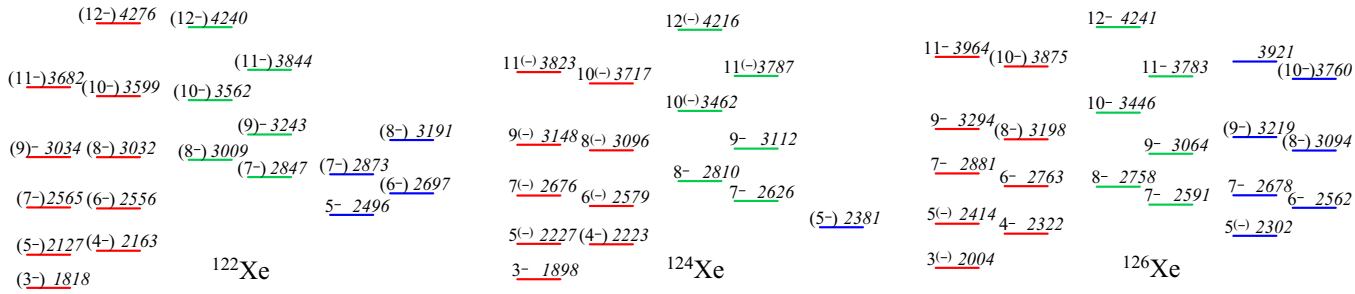

FIG. 19. Systematics of the negative-parity bands assigned in $^{122-126}$Xe. Data for ^{124}Xe are taken from Ref. [46], whereas those for ^{126,128}Xe are from Ref. [41].

Finally, Fig. 24 displays the alignment defined as

$$i(\omega) = I_x(\omega) - I_{x,ref}(\omega) \tag{8}$$

with $I_x = \sqrt{(I+\frac{1}{2})^2 - K^2}$ and the reference calculated using the moment of inertia defined by the Harris parameters, i.e., $I_{\rm ref} = (J_0 + J_2\omega^2)\omega$. The K values used were $K = 3$ for the 3^- band and its 4^- signature partner, and $K = 7$ for the 7^- band and its 8^- signature partner. While the values of the alignment are particularly sensitive to the choice of the Harris parameters, we note that the 3^- and 4^- signature partners have a continually increasing alignment with initial values of $2\hbar$–$3\hbar$ compared with the ground-state band, indicative of an octupole vibration. At $\hbar\omega \approx 200$ keV, the 3^- band has an increase in its alignment of $\simeq 2\hbar$ that tracks well with the ground-state band until the latter's back bend at $\hbar\omega \simeq 400$ keV. The 4^- signature partner, on the other hand, has an increasing alignment greater than that of the ground-state band below the back bend. This suggests a far more complicated structure in the octupole band, with an increasing influence of quasiparticle excitations with increasing spin with an accompanying decrease in the octupole collectivity. For completeness, the alignments for the 7^- and 8^- bands are also shown. Timmers *et al.* [45] suggest the $7/2[523] \otimes (1/2[411] + 5/2[402])$ two-quasineutron configuration for the low-spin parts of the 7^- and 8^- bands, that are crossed by the $(1/2[550])^2$ two-quasiproton alignment at $\hbar\omega \simeq 400$ keV. This crossing occurs over a rather wide range of frequency; however, below the crossing these bands also have an increasing alignment compared to the ground-state band.

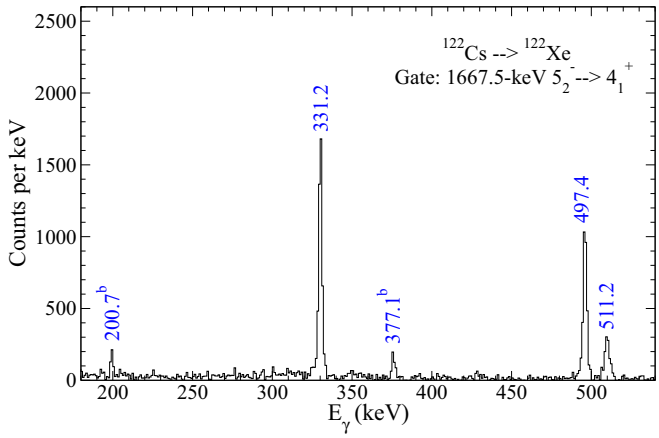

FIG. 20. Portion of the γ-ray spectrum observed with a coincidence condition the 1667.5 keV $5_2^- \rightarrow 4_1^+$ γ ray. Highlighted in the spectrum are the in-band transitions (superscript "b") feeding the 5_2^- level, as well as depopulating γ rays of the 4_1^+ level.

V. THEORETICAL RESULTS

A. Theoretical calculations

The results of the present experiment—precisely, for the positive-parity part of the spectrum—were interpreted with the aid of theoretical calculations as described in Ref. [14] (see also Refs. [48,49]). Briefly, the formalism used was that of the adiabatic time dependent Hartree-Fock-Bogoliubov (ATD-HFB) theory, leading to the construction of a collective Bohr-like Hamiltonian based on a microscopic mean-field input.

The general Bohr Hamiltonian has the advantage of acting in the full space of the quadrupole degrees of freedom and, in consequence, of treating simultaneously and on equal footing both vibrational and rotational excitations. Such a treatment is especially important for transitional nuclei. The "deformation" collective variables, β and γ, are defined as the mean

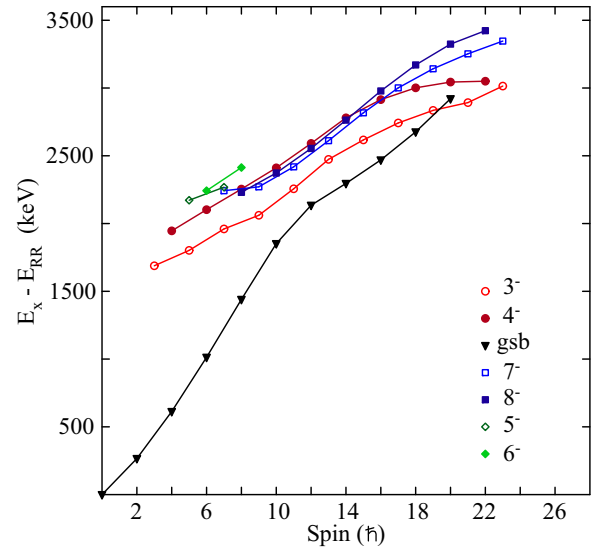

FIG. 21. Energies of the states in the ground state band (gsb), the $K^\pi = 3^-$ band, the $K^\pi = 7^-$ band, and the $K^\pi = 5^-$ band minus a rigid-rotor reference with $10.8I(I+1)$ keV.

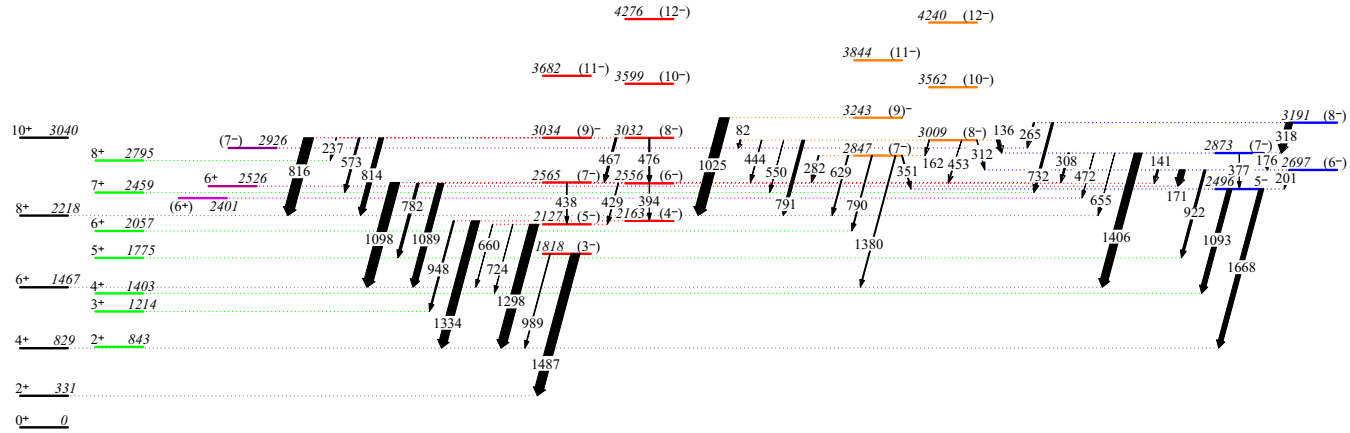

FIG. 22. Partial level scheme for ^{122}Xe showing the assigned negative-parity bands and their decays observed in the present work. Levels above spin 9^- were not observed in the present study.

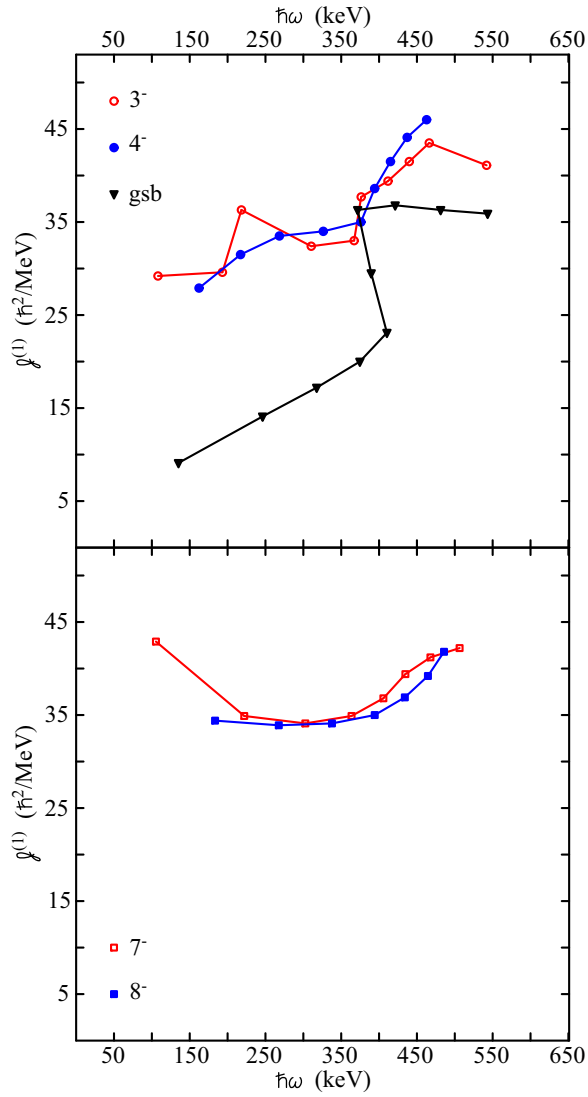

FIG. 23. The kinematic moment of inertia of the negative-parity bands, with the $K^\pi = 3^-$ band and the ground-state band, for reference, in the top panel, and the $K^\pi = 7^-$ band in the bottom panel.

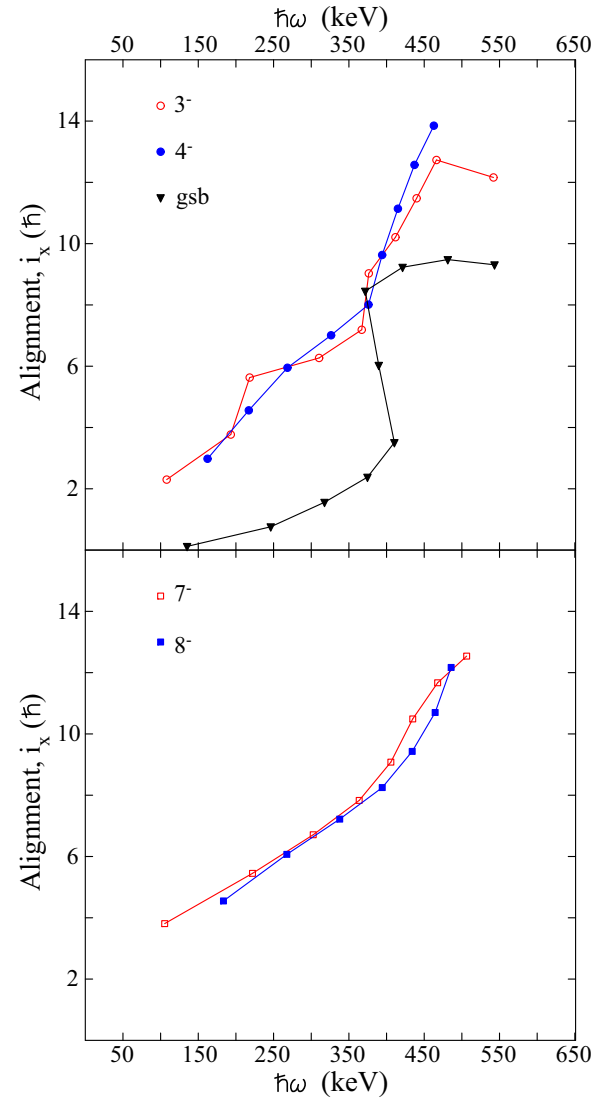

FIG. 24. Alignment extracted for the assigned negative-parity bands, with the 3^- and 4^- signature partners plotted together with the alignment for the ground-state band (top) and the 7^- and 8^- signature partners in the bottom panel.

values of components of the mass quadrupole tensor in the intrinsic frame,

$$Q_0 = \sum_{i=1}^{A} 3z_i^2 - r_i^2, \tag{9}$$

$$Q_2 = \sum_{i=1}^{A} \sqrt{3}\left(x_i^2 - y_i^2\right) \tag{10}$$

with

$$\beta \cos\gamma = c\langle\Phi|Q_0|\Phi\rangle, \tag{11}$$

$$\beta \sin\gamma = c\langle\Phi|Q_2|\Phi\rangle, \tag{12}$$

where $c = \sqrt{\pi/5}/A\bar{r^2}$ with $\bar{r^2} = 3/5r_0^2A^{2/3}$ and $r_0 = 1.2$ fm. Φ is a HFB wave function derived from, in the present case, the UNEDF0 energy density functional. The remaining three collective variables are the Euler angles Ω describing orientation of the intrinsic system relative to the laboratory frame.

The general Bohr Hamiltonian is determined by seven functions (potential energy V and six inertial functions which enter the kinetic energy part) and reads

$$H = T_{\rm vib} + T_{\rm rot} + V\ , \tag{13}$$

where

$$T_{\rm vib} = -\frac{1}{2\sqrt{wr}}\left\{\frac{1}{\beta^4}\left[\partial_\beta\left(\beta^4\sqrt{\frac{r}{w}}B_{\gamma\gamma}(\beta,\gamma)\partial_\beta\right) - \partial_\beta\left(\beta^3\sqrt{\frac{r}{w}}B_{\beta\gamma}(\beta,\gamma)\partial_\gamma\right)\right]\right.$$
$$\left. + \frac{1}{\beta\sin 3\gamma}\left[-\partial_\gamma\left(\sqrt{\frac{r}{w}}\sin 3\gamma B_{\beta\gamma}(\beta,\gamma)\partial_\beta\right) + \frac{1}{\beta}\partial_\gamma\left(\sqrt{\frac{r}{w}}\sin 3\gamma B_{\beta\beta}(\beta,\gamma)\partial_\gamma\right)\right]\right\}, \tag{14}$$

$$T_{\rm rot} = \frac{1}{2}\sum_{k=1}^{3} I_k^2/J_k, \quad J_k = 4\beta^2 B_k(\beta,\gamma)\sin^2(\gamma - 2k\pi/3), \tag{15}$$

$$V = V(\beta,\gamma), \tag{16}$$

and where

$$w = B_{\beta\beta}B_{\gamma\gamma} - B_{\beta\gamma}^2, \quad r = B_1B_2B_3. \tag{17}$$

In the formula (15), the operators I_k, $k = 1, 2, 3$ are components of the angular momentum in the intrinsic frame. The functions $B_{\beta\beta}, B_{\beta\gamma}, B_{\gamma\gamma}, B_k$ depend on deformation variables and are called mass parameters or, more precisely, inertial functions, while J_k are the moments of inertia. A volume element in the collective space is

$$d\tau_{\rm coll} = 2\sqrt{wr}\beta^4|\sin 3\gamma|d\beta\, d\gamma\, d\Omega, \tag{18}$$

where $d\Omega$ is the volume element in the Euler angles space.

The potential energy and the mass parameters for the collective Hamiltonian are calculated from the ATDHFB theory. All mass parameters were scaled by multiplying by a factor 1.3. This scaling can be considered as a very approximate way of inclusion of the so-called Thouless-Valatin correction coming from neglected time-odd parts of the mean field. It was shown in Ref. [14] that such a factor gave much better agreement with the excitation energies, but had a minor effect on the transition probabilities.

An important collective operator is the $E2$ quadrupole charge tensor which is determined from the microscopic theory as

$$q_{2\mu}^{\rm (charge)} = \langle\Phi|e\sum_{i=1}^{Z} r_i^2 Y_{2\mu}(\theta_i,\phi_i)|\Phi\rangle \tag{19}$$

where Φ is the same as in Eq. (11) and the sum extends over all protons. While the eigenfunctions of the Hamiltonian in Eq. (14) are known, the $E2$ operator of Eq. (19) is used to calculate $E2$ transition probabilities and quadrupole spectroscopic moments. No effective charge is used in Eq. (19).

We emphasize the following point: β and γ are dynamical variables and there is no fixed shape of the nucleus. Instead, we have only probability distributions determined by eigenfunctions of the Bohr Hamiltonian. An eigenfunction with the angular momentum numbers I, M and additional label ξ has the form

$$\Psi_{IM\xi}^{\rm (coll)}(\beta,\gamma,\Omega) = \sum_{K=0(2),\rm even}^{I\ \text{or}\ I-1} F_{IK\xi}(\beta,\gamma)\phi_{MK}^{I}(\Omega), \tag{20}$$

where

$$\phi_{MK}^{I} = \sqrt{\frac{2I+1}{16\pi^2(1+\delta_{I0})}}\left[D_{KM}^{I} + (-)^I D_{M-K}^{I}\right] \tag{21}$$

are normalized combinations of the Wigner D functions. The probability density function obtained by integration of $|\Psi^{\rm (coll)}|^2$ over the Euler angles reads

$$p_{I\xi}(\beta,\gamma) = \sum_{K}|F_{IK\xi}(\beta,\gamma)|^2\sqrt{wr}\beta^4|\sin 3\gamma|. \tag{22}$$

The probability density functions contain the weight function which enters the volume element, Eq. (18), in the collective space.

Figure 25 displays the potential energy surface (PES) for ^{122}Xe resulting from the calculations using the UNEDF0 energy density functional. As can be seen, the potential is rather soft in both the β and γ degrees of freedom, and thus the wave function distribution will not be strongly localized. While having a high degree of softness, the potential is asymmetric about the $\gamma = 30^\circ$ axis with a narrower potential in β on the

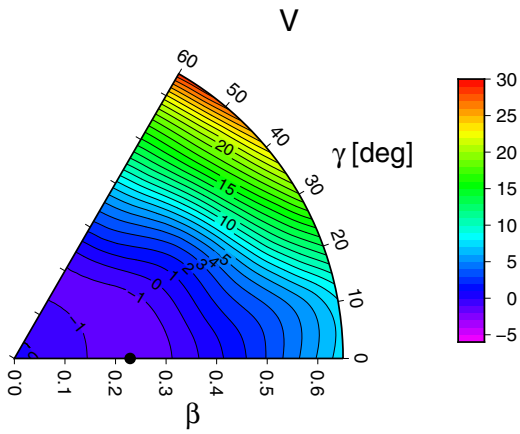

FIG. 25. Potential energy surface relative to a spherical shape value derived using the UNEDF0 energy density functional. The contours are at intervals of 1 MeV, with the minimum as a black dot located on the prolate axis at $\beta_2 = 0.23$. The potential is soft in both γ and β degrees of freedom.

oblate axis than on the prolate axis. In addition, the minimum of the PES decreases from $\simeq$0.23 on the prolate axis to $\simeq$0.16 on the oblate axis.

Figure 26 displays the wave function probability distributions in the (β, γ) plane [see Eq. (22)] for the first three 0^+ and 2^+ states. These will be discussed in more detail below, but we give a brief overview. The ground state and its 2_1^+ rotational band member have a triaxial shape, with $\beta \simeq 0.23$ and $\gamma \simeq 15^\circ$ for the 0_1^+ state, and with slightly larger β for the 2^+ state. The 2_2^+ state, which forms the head of a "$K = 2$" band, is a maximally triaxial state. The 0_2^+ state and its rotational band member, the 2_3^+ level, possess two lobes in their wave function distributions: a prolate lobe with $\beta \simeq 0.4$ and $\gamma \simeq 10^\circ$, and an oblate lobe with $\beta \simeq 0.18$ and $\gamma \simeq 50^\circ$. The wave function probability distributions have some similarity to that expected for a one-phonon γ vibration except that (1) the probability distributions strongly favor the prolate lobe, and (2) they are centered at significantly different values of β. This appearance reflects the observations of the PES above in that it was asymmetric about the $\gamma = 30^\circ$ line. Thus, while the 0_2^+ wave function has some characteristics of the one-phonon γ vibration, it is far from the idealized case and we can expect significant deviations from a typical γ-vibration behavior. The 2_3^+ level, the rotational band member of the 0_2^+ state, is even more strongly asymmetric in its wave function distribution, and bears little resemblance to a one-phonon γ vibration. The 0_3^+ state also possesses two lobes: the most probable is centered at $(\beta, \gamma) \simeq (0.22, 40^\circ)$, with the less-probable lobe centered at $(0.18, 5^\circ)$. The nodal line has both a β and γ dependence, in contrast to that for an idealized β vibration.

B. Interpretation of the theoretical results

The states and their decays calculated as described above were arranged into a series of rotational bands as depicted in Fig. 27. The transitions are labeled with their $B(E2)$ values in W.u., and for the sake of brevity, only those with $\geqslant$5 W.u. are shown. In the following discussion, we will use a labeling of a band by a K value, although this is signifying a sequence of states rather than an assertion that K is a good quantum number.

The weak dependence of the potential energy V on the γ variable suggests that the low-lying bands can be characterized in terms of the SO(5) irreps $[\nu, 0]$, which are eigenfunctions of the Wilets-Jean model, labeled with seniority ν with the understanding that it will only be an approximately conserved quantum number in the full calculation. The procedure for assigning the states is outlined in, for example, Refs. [50–52]. For each seniority ν, states of angular momentum L are given by the decomposition of the SO(5) irrep into the direct sum of SO(3) irreps with $L = 2k, 2k-2, 2k-3, \ldots, k$ with $k = \nu, \nu-3, \nu-6, \ldots, k_{\min}$ and $k_{\min} = 0$, 1, or 2. These states can be organized into bands with a bandhead of angular momentum K and rotational states of angular momentum $L = 0, 2, 4, \ldots$ for $K = 0$ and $L = K, K+1, K+2, \ldots$ for $K > 0$. The sequence of bands generated has $K = 0, 2, 4, 6, \ldots$ that have their bandheads at internals of $\Delta\nu = 2$, and moreover this set of K bands is also repeated at internals of $\Delta\nu = 3$. The lowest sequence of $K = 0, 2, 4, 6, \ldots$ bands are zero-vibrational-phonon states and coincide with those expected from a rigid triaxial rotor; the next sequence of $K = 0, 2, 4, 6, \ldots$ bands are one-γ-phonon vibrational states, etc. The $E2$ selection rules involve $\Delta\nu = \pm 1$ and $B(E2)$ values up to $\nu = 6$ are given in Ref. [51].

In the following discussion, we refer to both Figs. 26 and 27. The $K = 0$ ground-state band, whose wave function probability distribution displays a significant dispersion in the γ degree of freedom, has, in terms of the SO(5) irreps, increasing seniority $\Delta\nu = 1$ for each successive level. The 2_2^+ $K = 2$ bandhead at 741 keV is expected to be dominated by a seniority $\nu = 2$ component, with the spin 3 and 4 members having $\nu = 3$, the spin 5 and 6 members $\nu = 4$, etc. The spin 3 and 4 members of the $K = 2$ band can decay to the lower seniority 2 states, the 4_1^+ in the ground-state band and the $K = 2_1$ bandhead, and assuming SO(5) symmetry with $B(E2)$ values of 10/21, 25/21, 50/63, and 55/63, respectively, relative to the $B(E2; 2_1^+ \to 0_1^+)$ value. From the detailed calculations, the $B(E2)$ ratios are approximately 8/21, 28/21, 38/63, and 61/63. The 24 W.u. $4_2^+ \to 3_1^+$ transition indicates the breaking of the SO(5) symmetry as this transition should involve $\Delta\nu = 0$ and hence is forbidden. The $K = 4$ bandhead at 1805 keV belongs to this set of bands, and is a seniority $\nu = 4$ state with SO(5)-conserved $B(E2)$ values for decay to the $\nu = 3$ states of 26/26 (3_1^+), 910/1089 (4_2^+), and 64/3267 (6_1^+); the values from the detailed calculation are approximately 28/26, 849/1089, and 61/3267 (the latter is not shown on Fig. 27 due to its weakness), respectively. The $K = 6$ band is expected in the proximity of the 12^+ ($\nu = 6$) state of the ground-state band, and is beyond the range of the present calculations.

There are two 0^+ states predicted in the vicinity of 1 MeV: the 0_2^+ state at 905 keV, and the 0_3^+ state at 1271 keV. In the SO(5) limit, the one-phonon γ vibration should be degenerate with the other $\nu = 3$ states; from the energy consideration this would favor the 0_2^+ state, consistent with its wave function distribution although, as discussed above, it is not an idealized γ vibration. The $B(E2)$ values for the interband decay from the band members strongly favor the $K = 2_1$ band. With this

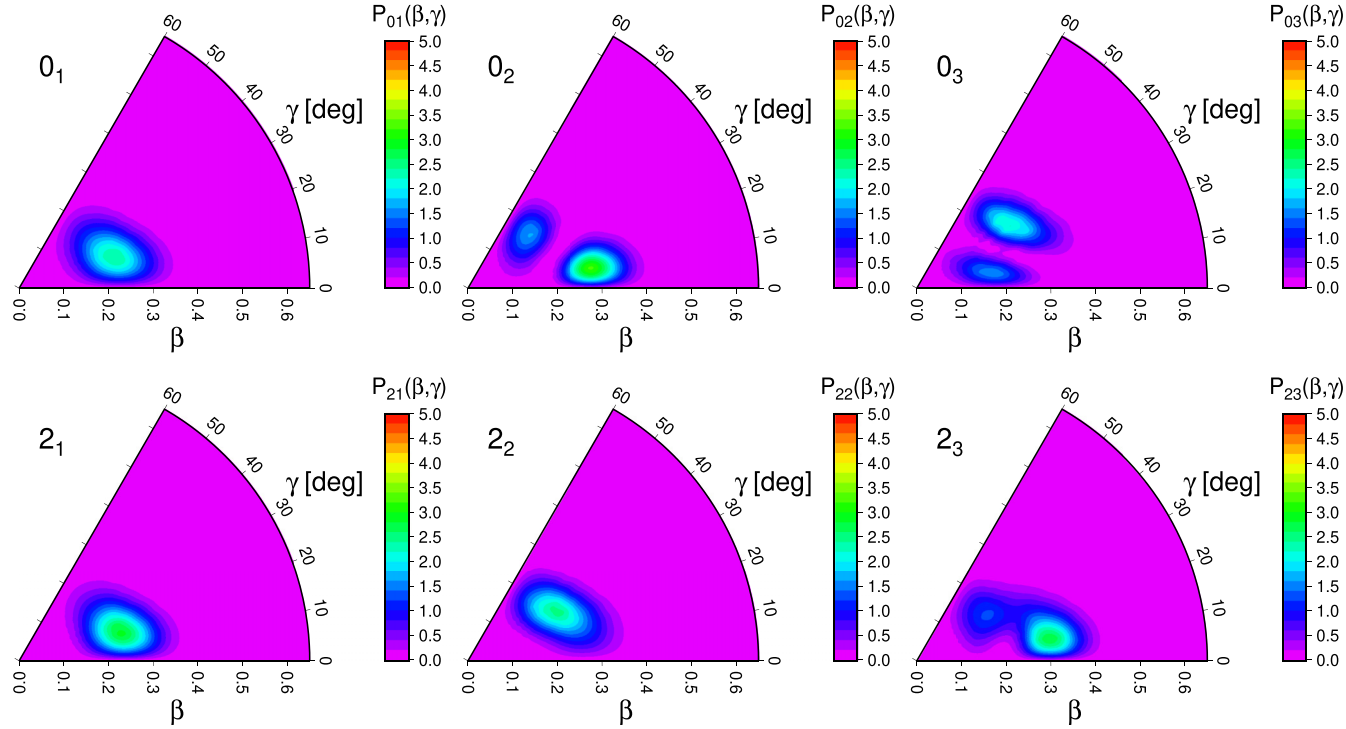

FIG. 26. Wave function probability distributions in the (β, γ) plane for the (a) 0_1^+, (b) 0_2^+, (c) 0_3^+, (d) 2_1^+, (e) 2_2^+, and (f) 2_3^+ states derived using the UNEDF0 energy density functional. See text for details.

assignment, the $K = 2$ one-γ-phonon state ($\nu = 5$) is the $K = 2_3$ bandhead at 1892 keV that has the enhanced $B(E2)$ value for decay to the 2^+ ($\nu = 4$) member of the $K = 0_2$ band and the $K = 4$ ($\nu = 4$) bandhead. The $K = 4$ one-γ-phonon band is expected in the excitation energy region of the 8^+ member of the 0_2^+ band, beyond the range of the current calculations.

The 0_3^+ state has some characteristics of a β vibration as discussed above. Such an excitation is expected within the current model, with a repeating pattern of $K = 0$, 2, 4, etc., bands present, beginning with SO(5) seniority $\nu = 0$ as above. In the limit of SO(5) symmetry being obeyed, the $\Delta\nu = \pm 1$ selection rule is enforced; the β-phonon $K = 0$ ($\nu = 0$) bandhead will decay to the $\nu = 1$ 2_1^+ state, the one-β phonon 2^+ ($\nu = 1$) state will decay to the 0_1^+ ground state, as well as the $\nu = 2$ 4_1^+ state and $K = 2_1$ bandhead, but not to the 2_1^+ state. The $K = 0_3$ band in Fig. 27 has only some of these characteristics, with only the bandhead possessing an enhanced $B(E2)$ value for decay to the $I + 2$ member of the ground-state band. All members of this band have strongly preferred decays to the $K = 2$ band, as would be expected for the one-phonon γ vibration. Thus, the 0_3^+ state also appears to follow some of the characteristics of the one-γ-phonon $K = 0$ state as well. Clearly, the 0_3^+ level is far from possessing a single, dominant SO(5) irrep in its wave function which causes a fragmentation of its decay. Regardless of the nature of the 0_3^+ band, Fig. 27 shows clearly that the third $K = 2$ band at 2231 keV is associated with the 0_3^+ state. The next bands, built on the 0_4^+ and 0_5^+ states, have complicated decay patterns that show the limitations of interpreting them within a SO(5)-conserving approach.

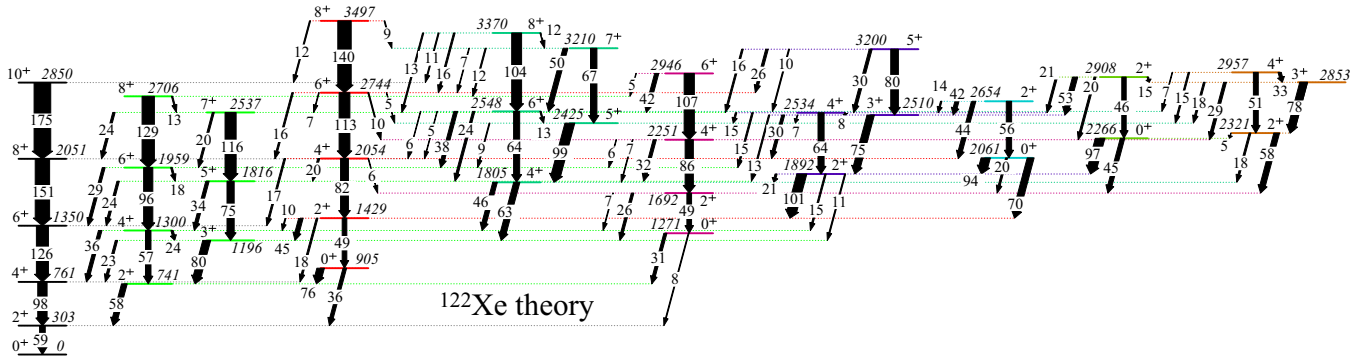

FIG. 27. Results of the theoretical calculations described in the text. The levels are arranged into bands according to their properties. The transitions are labeled with the $B(E2)$ values in W.u., and only those with values $\geqslant 5$ are shown.

TABLE III. Irreps of SO(5) with maximal probability (w_ν) for states in the g.s. and 2_2 bands. See text for more details.

	g.s. band				2_2 band			
Level	0_1	2_1	4_1	6_1	2_2	3_1	4_2	5_1
ν	0	1	2	3	2	3	3	4
w_ν	0.9	0.81	0.75	0.72	0.77	0.89	0.6	0.84

The above discussion can be augmented by decomposition of the wave functions obtained by numerical diagonalization of the Hamiltonian [Eq. (14)] into irreps of the SO(5) group. Table III contains a sample of results of such decomposition for the lowest levels of the g.s. and 2_2 band. For a given level a probability of the leading component, w_ν, and the corresponding seniority number ν is given. Generally, the SO(5) scheme works quite well for the lowest state for a given spin, but for higher states a significant mixing of the SO(5) irreps is observed. For example, for the 0_2 state we have $w_3 = 0.49$ and $w_0 = 0.41$ while for the 0_3 state $w_0 = 0.59$ and $w_3 = 0.32$.

VI. COMPARISON OF THE RESULTS

A. Comparison of $K = 0^+$ bands

The $B(E2)$ values for the ground-state band are shown on Fig. 28. The $B(E2)$ values for the decay of the 4^+ and 2^+ states are significantly larger than their theoretical counterparts, indicating that the degree of deformation in the calculations is underestimated. At higher spin, the calculated $B(E2)$ are larger than the experimental ones, which have large uncertainties.

As shown in Fig. 13, four excited 0^+ states are observed below 2.4 MeV, with the 2^+ band member assigned for the 0_2^+, 0_3^+, and 0_4^+ bands. The moments of inertia are very similar to that of the ground-state band, except for the 0_4^+ band where the 2^+ energy difference is 476.3 keV compared with 331.2 keV for the ground-state band. As displayed in Fig. 28, the relative $B(E2)$ values for the decay of the 0_2^+, 0_3^+, and 0_4^+ states favor decay to the $K^\pi = 2_1^+$ bandhead, with the preference for this decay increasing with excitation energy. The 0_5^+ state, however, has a much more fragmented decay, and its relative $B(E2)$ value strongly favors the decay to the 2^+ member of the 0_3^+ band. This highly unusual pattern implies that the wave functions have a large overlap, although the lack of absolute transition rates prevents definitive statements.

In the theoretical calculations, as shown in Fig. 27, four excited 0^+ states are also predicted below 2.4 MeV, at 905, 1271, 2061, and 2266 keV. The 0_2^+ and 0_3^+ states favor decay to the 2_2^+ bandhead, with the 0_4^+ state having an enhanced decay to both the 2^+ member of the 0_2^+ band, as well as the second $K^\pi = 2^+$ bandhead. We identify the experimental 0_2^+ state with the 0_2 state in the calculations, and note that relative $B(E2)$ ratios for the 0_2^+ bandhead are 100:32 (experimental) vs 100:47 (calculated) for decay to the 2_2^+ and 2_1^+ states. From the data given in Table I, the 2^+ band member at 1495.0 keV has $B(E2)$ values with a ratio of 100:12 for the in-band decay vs the decay to the 4_1^+ level, compared with the calculated ratio of 100:37. This is an excellent agreement considering the parameter-free nature of the calculations.

As discussed in Sec. I, the 0_3^+ state in the heavier Xe isotopes have enhanced populations in the two-proton pickup reactions that can be interpreted as evidence for a proton-pairing vibration nature. This degree of freedom is outside the current calculations, and, as demonstrated by Nomura *et al.* [27], can be important for the description of the low-lying excited 0^+ states. Based on the energy systematics, it is likely that the 0_3^+ level at 1716.5 keV in ^{122}Xe also has an significant contribution from the proton-pairing vibration. In ^{124}Xe, the 0_3^+ state has moderately enhanced $B(E2)$ values for decay

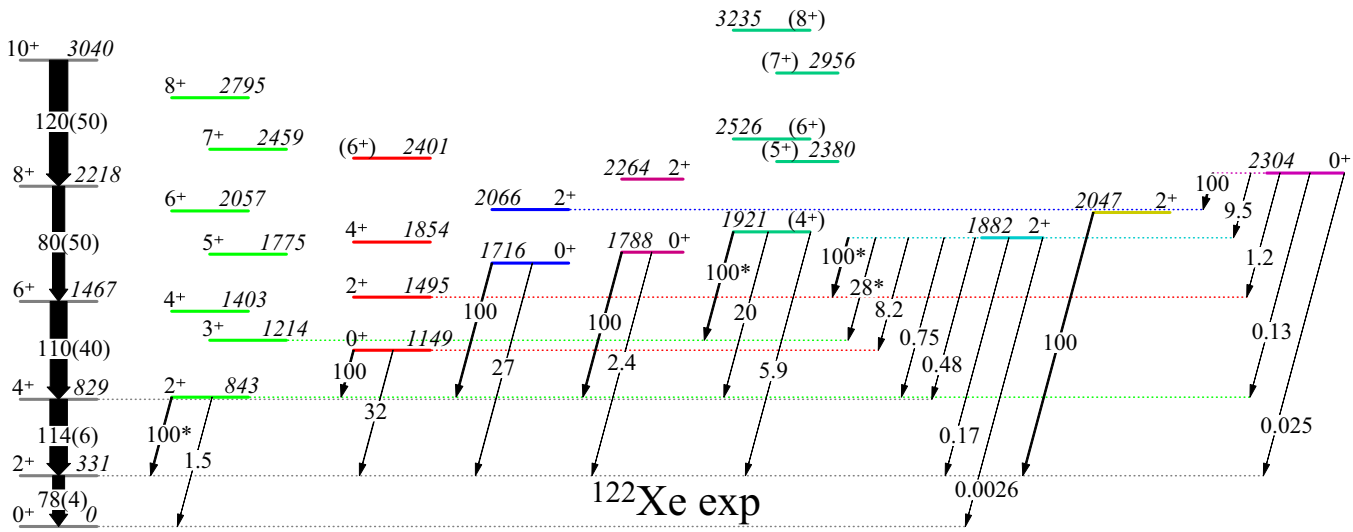

FIG. 28. Positive-parity bands assigned in the present study. The levels are arranged into bands based primarily on the presence of enhanced relative $B(E2)$ values for decay to lower-spin states. The transitions are labeled with their $B(E2)$ values in W.u. with the uncertainty in parenthesis for the ground-state band (taken from Ref. [17], and the other levels with their relative $B(E2)$ values normalized to 100 for the strongest branch. Those labeled with an asterisk assume a pure $E2$ multipolarity. For clarity, only the decays from the bandheads are shown.

to both the 2_1^+ and 2_2^+ levels of 11.9(17) and 9.2(14) W.u., respectively [19]. These values are significantly less than the values predicted for the 0_3^+ level, or any of the 0^+ states, in the present calculation. The 0_4^+ level is located at 1788.1 keV, and has a decay pattern consistent with the 0_3^+ state in the calculations predicted at 1271 keV. Unfortunately, the absolute $B(E2)$ values are unknown. At higher excitation energy, the 0_5^+ at 2304.0 keV has its largest relative $B(E2)$ value for the transition to the 2^+ band member of the 0_3^+ band. Due to the lack of absolute $B(E2)$ values, its nature cannot be ascertained.

B. Comparison of $K = 2^+$ bands

The 2_2^+ level at 843.2 keV is in excellent agreement with the 2_2^+ state predicted at 741 keV. As outlined above, in the calculations this is a zero-phonon state dominated by $\nu = 2$ SO(5) seniority component with the consequence that it strongly favors the decay to the 2_1^+ level, and this is reflected in the experimental data as well. The second $K = 2$ bandhead is assigned as the observed 2^+ state at 1882.0 keV. Its preferred decay, as seen in Fig. 28, is to the states in the 0_2^+ and 2_2^+ bands, in reasonable agreement with the predicted properties of the second $K = 2$ bandhead in the calculations that has the nature of the $K = 2$ state built on the 0_2^+ configuration. A higher-lying 2^+ state at 2047.0 is observed that has also been assigned as a $K = 2$ bandhead, but lack of details in its observed decay prevents a structural assignment. We note, however, that it is too low in energy to be associated as a $K = 2$ excitation on higher-lying 0^+ states, and may be a two-quasiparticle bandhead. Unfortunately, no absolute $B(E2)$ values are known, and thus detailed comparisons with the calculations regarding the collectivity cannot be performed.

C. Comparison of $K = 4^+$ band

A $K = 4$ band is assigned at 1920.6 keV which is in excellent agreement with the predicted energy of 1805 keV. As discussed above, in the calculations this is a zero-phonon $\nu = 4$ state with enhanced decays to the 3^+ and 4^+ members of the 2_2^+ band. Experimentally, the decay to the 4^+ member of the 2_2^+ state is not observed, whereas that to the 3^+ member is observed but with an unknown mixing ratio. Assuming that the transition to the 3^+ state is a pure $E2$ transition, its $B(E2)$ value would be a factor of 5 stronger than the decay to the 2_2^+ bandhead. It should be noted that the assigned 4^+ member of the 0_2^+ band at 1854.5 keV has a very similar decay pattern, perhaps indicating that these states are strongly mixed.

VII. SUMMARY

Excited states of ^{122}Xe have been investigated via β^+/EC decay of ^{122}Cs using the 8π γ-ray spectrometer at the TRIUMF Isotope Separator and Accelerator facility. The data were analyzed relying primarily on γ-γ coincidences, and γ-γ angular correlations were used to determine level spins and transition mixing ratios. The level of statistics achieved enabled the observation of 520 γ-ray transitions and 191 levels including eight new excited 0^+ states that were firmly assigned by the angular correlation analysis. The large number of excited 0^+ states observed and assigned rivals that of sensitive (p, t) transfer reactions—often the tool of choice to map the location of excited 0^+ states—and indicates that β decay should be considered whenever a parent state with an appropriate spin and Q value occurs.

A series of rotational bands have been assigned based on the spin-parities of the excited states, the γ-ray decay patterns, and extension of energy-level systematics from the heavier Xe isotopes. The $K^\pi = 0_2^+$ band has been tentatively extended to spin 6, and the 2^+ rotational band members of the 0_3^+ and 0_4^+ bands have been located. A new $K^\pi = 4^+$ band has been suggested, as well as the $K^\pi = 3^-$ and 5^- bands, with the 3^- band extended downwards from previously known higher-spin states. Firm assignments of the structures, however, must await measurements of the in-band transition rates.

The positive-parity bands have been compared to calculations based on the UNDEF0 energy density functional using the adiabatic time-dependent HFB formalism mapped to a Bohr-like Hamiltonian. The results are in good general agreement considering the parameter-free nature of the calculations. Unfortunately, more detailed tests of the calculations cannot be performed due to the limited amount of transition-rate data known for ^{122}Xe. Ideally, detailed Coulomb excitation measurements should be performed that could be within reach of the current generation of radioactive-beam facilities.

ACKNOWLEDGMENTS

This work was supported in part by the Natural Sciences and Engineering Research Council (Canada), TRIUMF through the National Research Council (Canada), and by the U.S. National Science Foundation under Grant No. PHY-1305801.

[1] M. J. Dolinski, A. W. P. Poon, and W. Rodejohann, Annu. Rev. Nucl. Part. Sci. **69**, 219 (2019).
[2] K. Blaum, S. Eliseev, F. A. Danevich, V. I. Tretyak, S. Kovalenko, M. I. Krivoruchenko, Y. N. Novikov, and J. Suhonen, Rev. Mod. Phys. **92**, 045007 (2020).
[3] G. Martínez-Lema, M. Martínez-Vara, M. Sorel, C. Adams, V. Álvarez, L. Arazi, I. J. Arnquist, C. D. R. Azevedo, K. Bailey, F. Ballester *et al.*, J. High Energ. Phys. 02 (2021) 203.
[4] D. R. Artusa, F. T. Avignone III, O. Azzolini, M. Balata, T. I. Banks, G. Bari, J. Beeman, F. Bellini, A. Bersani, M. Biassoni *et al.*, Adv. High Energy Phys. **2015**, 1 (2015).
[5] C. Alduino, F. Alessandria, K. Alfonso, E. Andreotti, C. Arnaboldi, F. T. Avignone, III, O. Azzolini, M. Balata, I. Bandac, T. I. Banks *et al.*, Phys. Rev. Lett. **120**, 132501 (2018).
[6] J. D. Vergados, H. Ejiri, and F. Šimkovic, Rep. Prog. Phys. **75**, 106301 (2012).
[7] J. Engel and J. Menéndez, Rep. Prog. Phys. **80**, 046301 (2017).

[8] P. von Brentano, A. Gelberg, S. Harissopulos, and R. F. Casten, Phys. Rev. C **38**, 2386 (1988).
[9] V. Werner, H. Meise, I. Wiedenhöver, A. Gade, and P. von Brentano, Nucl. Phys. A **692**, 451 (2001).
[10] G. Rainovski, N. Pietralla, T. Ahn, L. Coquard, C. J. Lister, R. V. F. Janssens, M. P. Carpenter, S. Zhu, L. Bettermann, J. Jolie *et al.*, Phys. Lett. B **683**, 11 (2010).
[11] H. von Garrel, P. von Brentano, C. Fransen, G. Friessner, N. Hollmann, J. Jolie, F. Käppeler, L. Käubler, U. Kneissl, C. Kohstall *et al.*, Phys. Rev. C **73**, 054315 (2006).
[12] L. Coquard, N. Pietralla, T. Ahn, G. Rainovski, L. Bettermann, M. P. Carpenter, R. V. F. Janssens, J. Leske, C. J. Lister, O. Möller *et al.*, Phys. Rev. C **80**, 061304 (2009).
[13] J. B. Gupta, Nucl. Phys. A **927**, 53 (2014).
[14] L. Próchniak, Phys. Scr. **90**, 114005 (2015).
[15] W. P. Alford, R. E. Anderson, P. A. Batay-Csorba, R. A. Emigh, D. A. Lind, P. A. Smith, and C. D. Zafiratos, Nucl. Phys. A **323**, 339 (1979).
[16] K. Kitao, Y. Tendow, and A. Hashizume, Nucl. Data Sheets **96**, 241 (2002).
[17] T. Tamura, Nucl. Data Sheets **108**, 455 (2007).
[18] J. Katakura and Z. D. Wu, Nucl. Data Sheets **109**, 1655 (2008).
[19] A. J. Radich, P. E. Garrett, J. M. Allmond, C. Andreoiu, G. C. Ball, L. Bianco, V. Bildstein, S. Chagnon-Lessard, D. S. Cross, G. A. Demand *et al.*, Phys. Rev. C **91**, 044320 (2015).
[20] H. Iimura, J. Katakura, and S. Ohya, Nucl. Data Sheets **180**, 1 (2022).
[21] Z. Elekes and J. Timar, Nucl. Data Sheets **129**, 191 (2015).
[22] B. Singh, Nucl. Data Sheets **93**, 33 (2001).
[23] K. Heyde and J. L. Wood, Rev. Mod. Phys. **83**, 1467 (2011).
[24] H. W. Fielding, R. E. Anderson, P. D. Kunz, D. A. Lind, C. D. Zafiratos, and W. P. Alford, Nucl. Phys. A **304**, 520 (1978).
[25] P. E. Garrett, J. Phys. G: Nucl. Part. Phys. **43**, 084002 (2016).
[26] P. E. Garrett, A. J. Radich, J. M. Allmond, C. Andreoiu, G. C. Ball, P. C. Bender, L. Bianco, V. Bildstein, H. Bidaman, R. Braid *et al.*, J. Phys.: Conf. Ser. **639**, 012006 (2015).
[27] K. Nomura, D. Vretenar, Z. P. Li, and J. Xiang, Phys. Rev. C **102**, 054313 (2020).
[28] B. Jigmeddorj, P. E. Garrett, C. Andreoiu, G. C. Ball, T. Bruhn, D. S. Cross, A. B. Garnsworthy, G. Hackman, B. Hadinia, M. Moukaddam *et al.*, EPJ Web Conf. **107**, 03014 (2016).
[29] P. E. Garrett, B. Jigmeddorj, A. D. MacLean, H. Bidaman, V. Bildstein, C. Burbadge, G. A. Demand, A. Daiz Varela, M. Dunlop, R. Dunlop *et al.*, Acta Phys. Pol. B **48**, 523 (2017).
[30] B. Jigmeddorj, P. E. Garrett, C. Andreoiu, G. C. Ball, T. Bruhn, D. S. Cross, A. B. Garnsworthy, B. Hadinia, M. Moukaddam, J. Park *et al.*, Phys. Procedia **90**, 435 (2017).
[31] B. Jigmeddorj, P. E. Garrett, C. Andreoiu, G. C. Ball, T. Bruhn, D. S. Cross, A. B. Garnsworthy, B. Hadinia, M. Moukaddam, J. Park *et al.*, EPJ Web Conf. **178**, 02026 (2018).
[32] A. B. Garnsworthy and P. E. Garrett, Hyperfine Interact. **225**, 121 (2014).
[33] A. B. Garnsworthy *et al.*, E. Phys. J. Web of Conf. **93**, 01032 (2015).
[34] P. E. Garrett *et al.*, Nucl. Instrum. Methods Phys. Res., Sect. B **261**, 1084 (2007).
[35] B. Jigmeddorj, P. E. Garrett, A. Diaz Varela, G. C. Ball, J. C. Bangay, D. S. Cross, G. A. Demand, A. B. Garnsworthy, K. L. Green, K. G. Leach *et al.*, JPS Conf. Proc. **6**, 030014 (2015).
[36] D. C. Radford, RadWare software repository maintained at http://radware.phy.ornl.gov
[37] See Supplemental Material at http://link.aps.org/supplemental/10.1103/PhysRevC.110.024305 for the decay schemes of the $^{122}Cs^{gs}$ and $^{122}Cs^{m}$ and all the γ-γ angular correlations extracted.
[38] W. D. Kulp, J. L. Wood, J. M. Allmond, J. Eimer, D. Furse, K. S. Krane, J. Loats, P. Schmelzenbach, C. J. Stapels, R.-M. Larimer, E. B. Norman, and A. Piechaczek, Phys. Rev. C **76**, 034319 (2007).
[39] P. E. Garrett, J. Bangay, A. Diaz Varela, G. C. Ball, D. S. Cross, G. A. Demand, P. Finlay, A. B. Garnsworthy, K. L. Green, G. Hackman *et al.*, Phys. Rev. C **86**, 044304 (2012).
[40] A. J. Radich, P. E. Garrett, J. M. Allmond, C. Andreoiu, G. C. Ball, L. Bianco, V. Bildstein, S. Chagnon-Lessard, D. S. Cross, A. Diaz Varela *et al.*, JPS Conf. Proc. **6**, 030015 (2015).
[41] https://www.nndc.bnl.gov/logft/
[42] H. J. Rose and D. M. Brink, Rev. Mod. Phys. **39**, 306 (1967).
[43] P. Schmelzenbach, Ph.D. thesis, Oregon State University, 2003.
[44] A. Gade, I. Wiedenhover, J. Gableske, A. Gelberg, H. Meise, N. Pietralla, and P. von Brentano, Nucl. Phys. A **665**, 268 (2000).
[45] H. Timmers, J. Simpson, M. A. Riley, T. Bengtsson, M. A. Bentley, F. Hannat, S. M. Mullins, J. F. Sharpey-Schafer, and R. Wyss, J. Phys. G: Nucl. Part. Phys. **20**, 287 (1994).
[46] A. J. Radich, P. E. Garrett, L. Próchniak, C. Andreoiu, G. C. Ball, L. Bianco, V. Bildstein, S. Chagnon-Lessard, D. S. Cross, G. A Demand *et al.* (private communication).
[47] W. F. Mueller, M. P. Carpenter, J. A. Church, D. C. Dinca, A. Gade, T. Glasmacher, D. T. Henderson, Z. Hu, R. V. F. Janssens, A. F. Lisetskiy, C. J. Lister, E. F. Moore, T. O. Pennington, B. C. Perry, I. Wiedenhöver, K. L. Yurkewicz, V. G. Zelevinsky, and H. Zwahlen, Phys. Rev. C **73**, 014316 (2006).
[48] L. Próchniak and S. G. Rohoziński, J. Phys. G: Nucl. Part. Phys. **36**, 123101 (2009).
[49] K. Wrzosek-Lipska, L. Próchniak, M. Zielińska, J. Srebrny, K. Hadynska-Klek, J. Iwanicki, M. Kisielinski, M. Kowalczyk, P. J. Napiorkowski, D. Pietak, and T. Czosnyka, Phys. Rev. C **86**, 064305 (2012).
[50] D. J. Rowe and J. L. Wood, *Fundamentals of Nuclear Models: Foundational Models* (World Scientific, Singapore, 2010).
[51] D. J. Rowe, Nucl. Phys. A **735**, 372 (2004).
[52] D. J. Rowe, P. S. Turner, and J. Repka, J. Math. Phys. **45**, 2761 (2004).